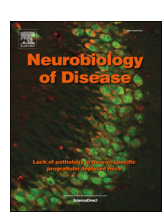
FISEVIER

Contents lists available at ScienceDirect

### Neurobiology of Disease

journal homepage: www.elsevier.com/locate/ynbdi



# A Christianson syndrome-linked deletion mutation ( $\Delta 287ES288$ ) in *SLC9A6* impairs hippocampal neuronal plasticity



Andy Y.L. Gao<sup>a</sup>, Alina Ilie<sup>b</sup>, Philip K.Y. Chang<sup>c</sup>, John Orlowski<sup>b</sup>, R. Anne McKinney<sup>c,d,\*</sup>

- <sup>a</sup> Integrated Program in Neuroscience, McGill University, Montreal, QC, Canada
- <sup>b</sup> Departments of Physiology, McGill University, Montreal, QC, Canada
- <sup>c</sup> Pharmacology & Therapeutics, McGill University, Montreal, QC, Canada
- <sup>d</sup> Neurology & Neurosurgery, McGill University, Montreal, QC, Canada

#### ARTICLE INFO

#### Keywords: SLC9A6/NHE6 Christianson syndrome AMPA receptors Plasticity Endosomes X-linked intellectual disability Organellar pH

#### ABSTRACT

Christianson Syndrome is a rare but increasingly diagnosed X-linked intellectual disability disorder that arises from mutations in SLC9A6/NHE6, a pH-regulating transporter that localizes to early and recycling endosomes. We have recently reported that one of the originally identified disease-causing mutations in NHE6 (p.E287-S288del, or ΔES) resulted in a loss of its pH regulatory function. However, the impact of this mutation upon neuronal synapse formation and plasticity is unknown. Here, we investigate the consequences of the  $\Delta$ ES mutant upon mouse hippocampal pyramidal neurons by expressing a fluorescently-labeled ΔES NHE6 construct into primary hippocampal neurons. Neurons expressing the ΔES mutant showed significant reductions in mature dendritic spine density with a concurrent increase in immature filopodia. Furthermore, compared to wild-type (WT), AES-containing endosomes are redirected away from early and recycling endosomes toward lysosomes. In parallel, the  $\Delta$ ES mutant reduced the trafficking of glutamatergic AMPA receptors to excitatory synapses and increased their accumulation within lysosomes for potential degradation. Upon long-term potentiation (LTP), neurons expressing ΔES failed to undergo significant structural and functional changes as observed in controls and WT transfectants. Interestingly, synapse density and LTP-induced synaptic remodeling in ΔES-expressing neurons were partially restored by bafilomycin, a vesicular alkalinisation agent, or by leupeptin, an inhibitor of lysosomal proteolytic degradation. Overall, our results demonstrate that the ΔES mutation attenuates synapse density and structural and functional plasticity in hippocampal neurons. These deficits may be partially due to the mistargeting of AMPA receptors and other cargos to lysosomes, thereby preventing their trafficking during synaptic remodeling. This mechanism may contribute to the cognitive learning deficits observed in patients with Christianson Syndrome and suggests a potential therapeutic strategy for treatment.

Abbreviations: (RS)-CPP, (RS)-3-(2-carboxypiperazin-4-yl)-propyl-1-phosphonic acid; AD, Alzheimer's disease; AF-Tfn, AlexaFluor633-tagged transferrin; AMPAR, α-amino-3-hydroxy-5-methyl-4-isoxazolepropionic acid receptor; ANOVA, analysis of variance; AP-1, Chinese hamster ovary (CHO) cells deficient in the Na<sup>+</sup>/H<sup>+</sup> antiporter 1 isoform; AP2, adaptor protein 2; APP, amyloid precursor protein; Arc, activity-regulated cytoskeleton-associated protein; Aβ, amyloid beta; BACE1, β-secretase 1; BDNF, brain-derived neurotrophic factor; CS, Christianson syndrome; DIV, day in vitro; DMEM, Dulbecco's Modified Eagle's Medium; DNA, deoxyribonucleic acid; EEA1, early endosomal antigen-1; EGFP, enhanced green fluorescent protein; EGTA, ethylene glycol-bis(β-aminoethyl ether)-N,N,N',N'-tetraacetic acid; FBS, fetal bovine serum; FGF1, fibroblast growth factor receptor 1; gly-ChemLTP, glycine-mediated chemical long-term potentiation; HA, influenza virus hemagglutinin epitope; HBSS, Hank's Balanced Salt Solution; HEK-293, human embryonic kidney 293 cells; HEPES, 4-(2-hydroxyethyl)-1-piperazineethanesulfonic acid; KO, knock-out; LAMP1, lysosomal-associated membrane protein 1; leu, leupeptin; LRP1, lipoprotein-related receptor protein 1; mCh, mCherry fluorescent protein; mEPSC, miniature excitatory postsynaptic current; MES, 2-(4-morpholino) ethanesulfonic acid; nACSF, normal artificial cerebrospinal fluid; NHE6/SLC9A6, sodium/proton exchanger isoform 6; NMDAR, N-methyl p-aspartate receptor; PCR, polymerase chain reaction; PD, post-natal day; PSD, post-synaptic density; SEP, superecliptic pHluorin; sGluA1, surface SEP-GluA1; SHV, spine head volume; Stx-13, syntaxin-12/13; tdT, tdTomato fluorescent protein; TrkB, tropomyosin receptor kinase B; UBE3A, ubiquitin-protein ligase E3A; WT, wild-type; ΔES, in-frame deletion mutation of amino acid residues glutamic acid 277 and serine 278 in NHE6

<sup>\*</sup>Corresponding author at: Life Sciences Complex, Bellini, 3649 Prom. Sir-William-Osler, Room 167, Montreal, QC H3G 0B1, Canada. *E-mail addresses*: andy.gao@mail.mcgill.ca (A.Y.L. Gao), alina.ilie@mcgill.ca (A. Ilie), philip.chang@mcgill.ca (P.K.Y. Chang),

#### 1. Introduction

Genetic or environmental mediated disturbances in early brain growth and maturation result in a heterogeneous group of neurodevelopmental disorders that can manifest as deficits in learning ability and memory, language and communication skills, emotion or motor coordination, amongst other behaviours. A recent addition to this spectrum of disorders is Christianson Syndrome (CS), an X-linked condition that becomes apparent in infancy and is characterized by moderate to severe intellectual disability, epilepsy, non-verbalism, ataxia, and autism-like behaviours (Christianson et al., 1999; Pescosolido et al., 2014; Schroer et al., 2010). These patients also undergo further deterioration in their symptoms, namely in cerebellar atrophy and Purkinie cell loss associated with a progressive loss of mobility after the first decade of life (Christianson et al., 1999; Gilfillan et al., 2008; Pescosolido et al., 2014). The frequency of CS is estimated at 1 in 16,000 to 1 in 100,000 people worldwide, which ranks it amongst the more common forms of X-linked intellectual disability (Tarpey et al., 2009). At present, however, the molecular mechanisms underlying CS are poorly understood, and effective interventions are lacking. CS results from mutations in the solute carrier gene SLC9A6 located at chromosome position Xq26.3, which encodes the electroneutral alkali cation (Na+, K+)/proton (H+) exchanger isoform 6 (commonly referred to as NHE6) (Orlowski and Grinstein, 2011). Slc9a6/Nhe6 knockout (KO) mice exhibit many of the symptoms observed in human, including reductions not only in cerebellar but also cortical and hippocampal volume with age, suggestive of broad neural degeneration (Xu et al., 2017).

The NHE6 gene is transcribed in most tissues but is especially abundant in brain (Deane et al., 2013), which likely accounts for the pronounced neuropathological appearance of CS. In neurons and other cell types, NHE6 localizes primarily to the membranes of early and recycling endosomes (Brett et al., 2002; Deane et al., 2013) and acts as a H<sup>+</sup> extrusion mechanism to moderate luminal acidification driven by the electrogenic vacuolar H+-ATPase pump (Xinhan et al., 2011). This is an important regulatory process, as endosomes carrying cargo intended for either recycling to the plasma membrane or degradation in lysosomes experience an increase or decrease in luminal pH, respectively. Indeed, graded acidification of endomembrane compartments along the recycling and degradative pathways is an important determinant of their biogenesis, trafficking and function (Casey et al., 2010; Paroutis et al., 2004; Weisz, 2003; Yamashiro and Maxfield, 1984). While the significance of this phenomenon has long been appreciated in non-neuronal cells, its impact on neuronal function is less well studied. Endosomal transport of lipids and membrane receptors, such as the neurotrophin tropomyosin receptor kinase B (TrkB) and glutamatergic α-amino-3-hydroxy-5-methyl-4-isoxazolepropionic acid receptors (AMPARs), is essential for axonal and dendritic development, synaptogenesis, and plasticity mechanisms (Chater and Goda, 2014; Numakawa et al., 2010; Overly and Hollenbeck, 1996). Thus, further investigation into the role of endosomal pH- and NHE6 in particular - in the optimal function and maintenance of neurons is warranted.

Our current understanding of how mutations in *NHE6* alter neuronal function in the pathophysiology of CS is limited. To date, over 50 *de novo* and inherited mutations in *SLC9A6* have been reported in CS patients (Garbern et al., 2010; Gilfillan et al., 2008; Pescosolido et al., 2014; Takahashi et al., 2011) (also see the databases ClinVar (https://www.ncbi.nlm.nih.gov/clinvar/) and DECIPHER (https://decipher.sanger.ac.uk/)). Many of these mutations truncate the protein in the transmembrane ion translocation domain, leading to a complete loss of function (Pescosolido et al., 2014). Previous experimental studies have focused mainly on an *Nhe6* knock-out (KO) mouse, in which endosomallysosomal function is impaired in neurons across various brain regions (Strømme et al., 2011). In hippocampal neurons prepared from *Nhe6* KO mice, axodendritic branching and the density of mature excitatory synapses is reduced compared to wild-type (WT) neurons (Ouyang

et al., 2013). While these experiments provide valuable insight into the consequences of the complete loss of NHE6 protein, it is unclear if these changes are mirrored in neurons expressing other disease-causing NHE6 mutants that generate an intact protein. Importantly, how disease-causing mutants may affect receptor trafficking and plasticity mechanisms, which could underlie the severe learning deficits observed in CS patients, is currently unknown.

We recently reported that an in-frame deletion mutant of NHE6 (NM\_001042537.1:c.860\_865delAAAGTG:p.E287\_S288del, referred to as  $\Delta$ ES) resulted in excess acidification of NHE6-containing endosomes and elicited significant reductions in dendritic arborization of primary cultures of transfected mouse hippocampal neurons (Ilie et al., 2016). In this report, we further investigate the effects of the  $\Delta$ ES mutant on excitatory synaptic density, AMPA receptor (AMPAR) trafficking and synaptic plasticity. Specifically, expression of the  $\Delta$ ES mutant in primary hippocampal neurons results in a reduction of dendritic spine density and impaired functional and structural spine remodeling in response to glycine-mediated chemically-induced long-term potentiation (i.e., gly-ChemLTP stimulation). We also show that the  $\Delta$ ES mutant is mislocalized within cells when compared to WT and disrupts the trafficking of glutamatergic AMPARs. Interestingly, treating ΔES-expressing neurons with either a lysosomal inhibitor or a vesicular alkalization agent partially rescues neuronal structure and plasticity. Our results highlight a critical role for NHE6 in synaptic morphology, remodeling and excitatory synaptic potentiation in hippocampal neurons, providing new mechanistic insight into some of the cognitive impairments associated with CS. In addition, NHE6 dysfunction has been implicated in the progression of other neurodegenerative disorders (Prasad and Rao, 2015; Schwede et al., 2013; Verma et al., 2015; Zhao et al., 2016). Hence, our findings may be relevant to a broader number of neuropathological conditions than previously realized.

#### 2. Methods

#### 2.1. Recombinant DNA constructs and mutagenesis

The long transcript splice-variant of human NHE6 (NHE6v1; NCBI refseq NM\_001042537) was cloned from a human brain Matchmaker™ cDNA library (Clontech) using PCR methodology and was engineered to contain the influenza virus hemagglutinin (HA) (YPYDVPDYAS) epitope at its extreme C-terminal end. This construct was termed wild-type NHE6-HA (NHE6WT-HA) and inserted into the HindIII and XbaI sites of the mammalian expression vector pcDNA3 (Invitrogen), as described previously (Ilie et al., 2014). NHE6-HA was then used as a template to engineer the double deletion mutation of amino acids E287 and S288 ( $\Delta E287/S288$ ,  $\Delta ES$ ) by PCR mutagenesis. mCherry fluorescent protein (mCh) C-terminal-tagged forms of NHE6 WT and  $\Delta$ ES mutant were constructed by insertion between the XhoI and HindIII restriction sites of the pAcGFP1-N1 vector (BD Biosciences Clontech, Palo Alto, CA). Insertion of the different epitope tags in the various positions did not alter the biochemical properties or cellular distribution of exogenous NHE6 compared to the endogenous protein (Ilie et al., 2016; Ilie et al., 2014). All constructs were sequenced to ensure that no additional mutations were introduced during PCR.

#### 2.2. Mouse primary hippocampal cultures

In vitro experiments were performed on primary hippocampal cultures prepared from early postnatal C57BL/6 mice, prepared as previously described (Brewer and Torricelli, 2007; Deane et al., 2013). In brief, post-natal day (PD) 0–1 mice pups were decapitated, their brains removed, and the hippocampi dissected out. These hippocampi were maintained in chilled HBSS supplemented with 0.1 M HEPES buffer and 0.6% glucose, then digested with 165 U papain for 20 min in a shaking water bath at 37 °C. Neurons and glia were dissociated by trituration and suspended in DMEM supplemented with 1% penicillin-

streptomycin, 10% FBS, and 0.6% glucose. Cells were then plated onto poly-D-lysine-coated 10 mm coverslips at an approximate density of 12,000 cells/cm² and placed in an incubator at 37 °C. 24 h later, plating media was replaced with Neurobasal-A growth media supplemented with 2% B-27 supplement, 1% GlutaMAX, and 1% penicillin-streptomycin. Cultures were then fed every 3–4 d and allowed to mature until 14+ days in vitro (DIV) at 37 °C in a humidified environment of 5% CO<sub>2</sub>. Over the course of this time period, these cells develop and form a functional neuronal network in a controlled manner (Potter and DeMarse, 2001).

#### 2.3. Calcium phosphate transfection

Primary neurons were transfected via calcium phosphate transfection as previously described (Jiang and Chen, 2006). In summary, at 11-12 DIV, coverslips were transferred into a 35 mm dish filled with warmed preconditioned growth media. Four micrograms of DNA plasmids were mixed with 50 µl 250 mM CaCl2 solution, which was next added to 50 µl 2× HEPES-buffered phosphate solution to form DNAtagged calcium phosphate precipitate. This was then added dropwise to each dish of coverslips and incubated at 37 °C in a humidified environment of 3% CO2 for 90 min. Prior to returning them to their original plates, 80 µl of sterile 0.3 M 2-(4-morpholino) ethanesulfonic acid (MES) acid buffer (pH 5.5) were added to each dish, which acidified the media to dissolve any remaining precipitate. The cultures were then maintained at 37 °C, 5%  $CO_2$  for  $\geq$  48 h before being further processed. In these experiments, we will mostly focus on the longest splice variant of NHE6, NHE6v1 (i.e., p.E287\_S288del in NHE6v1, or NHE6  $\Delta ES$  ). Cultures were generally co-transfected with plasmids encoding enhanced green fluorescent protein (EGFP) or tdTomato (to mark neuronal structure) and mCherry alone (as a transfection control) or either WT or ΔES NHE6 tagged to mCherry or influenza virus hemagglutinin epitope (HA). In surface GluA1 experiments, a construct encoding the AMPAR subunit GluA1 with N-terminally fused pH-sensitive superecliptic pHluorin (SEP-GluA1, gift from Dr. Edward Ruthazer) is utilized.

#### 2.4. Glycine-mediated chemical LTP

Glycine-mediated chemical long-term potentiation (gly-ChemLTP) was performed on primary hippocampal cultures as previously described (Deane et al., 2013; Fortin et al., 2010). To summarize, transfected neurons at 14+ DIV were placed into a heated (30 °C) recording chamber of an upright microscope (DM LFSA, Leica Microsystems, Heidelberg, Germany). Cultures were first perfused continuously for 15 min with normal artificial CSF (nASCF) containing the following (in mM): 125 NaCl, 2.5 KCl, 2 CaCl<sub>2</sub>, 1 MgCl<sub>2</sub>·6H<sub>2</sub>O, 5 HEPES, and 33 D (+)-glucose, pH 7.3, osmolarity 290 mOsmol/L, and gassed with 95% O<sub>2</sub>/5% CO<sub>2</sub>. The nACSF was then replaced with a stimulating solution of Mg<sup>2+</sup>-deficient ACSF with the following (in mM): 125 NaCl, 2.5 KCl, 2 CaCl<sub>2</sub>·2H<sub>2</sub>O, 5 HEPES, 33 D(+)-glucose, 0.2 glycine, 0.02 (-)-bicuculline methochloride, and 0.003 strychnine hydrochloride. After 10 min, neurons were be reperfused with nACSF for 20 min. To confirm that this phenomenon is NMDA receptor-dependent, this protocol was repeated in NHE6 WT-transfected cultures pretreated with (RS)-3-(2carboxypiperazin-4-yl)-propyl-1-phosphonic acid ((RS)-CPP; 50 μM), a competitive antagonist of the NMDA receptor, for 15 min prior to gly-ChemLTP stimulation. This antagonist was also included in the stimulation solution (gly-ChemLTP + CPP).

#### 2.5. Immunofluorescence

Primary cultures were fixed with 4% PFA/0.1 M PB, pH 7.4 (Sigma Aldrich) for 15 min at room temperature and washed with 0.1 M PB. Immunoprocessed cultures were first permeabilized for 1 min in 0.2% Triton X-100/0.1 M PB and blocked for 1 h at room temperature in 0.2%

Triton X-100/1% HIHS/0.1 MPB, before being incubated with primary antibodies (GFP 1:1000, Stx-13 1:500, EEA1 1:1000, Rab7: 1:500, LAMP1: 1:500, GluA1 1:200) diluted in blocking solution overnight at 4°C. After subsequent washing, cells were incubated with secondary antibody (Alexa Fluor 488, Alexa Fluor 594, Alexa Fluor 647, Dylight649 1:1000) for 45 min at room temperature and washed again. For analysis of NHE6 colocalization with soluble transferrin, live primary neurons were incubated with AF-Tfn (100  $\mu g/ml$ ) for 1 h at 37 °C and then fixed. For the analysis of surface SEP-GluA1 (sGluA1), transfected coverslips were subjected to the previously described gly-ChemLTP solution for 10 min in their native plate in a bead bath warmed to 37 °C and gassed with 95% O<sub>2</sub>/5% CO<sub>2</sub>. Afterwards, the stimulation solution was replaced with nASCF for a further 20 min before being incubated live with mouse GFP primary antibody diluted in nASCF (1:1000) for 1 h at 4 °C to prevent receptor internalization. Treated cultures were then fixed, washed, blocked, and stained with goat anti-mouse Dylight 649 secondary antibody under non-permeabilizing conditions (to stain the surface fraction of SEP-GluA1 only) before permeabilization and further immunoprocessing as previously described. This procedure was repeated with neurons pre-treated with CPP and subjected to gly-ChemLTP + CPP solution. All fixed coverslips were mounted onto SuperFrost (Menzel-Glaser) microscope slides using UltraMount fluorescence mounting medium (Dako) and left to dry overnight at room temperature in the dark.

#### 2.6. Electrophysiology

Forty-eight hours following transfection, cultures were placed into the recording chamber of an upright microscope (BX51WI, Olympus, XLUMPlanF1  $20 \times 0.95$  NA water immersion objective) and placed in consistent perfusion of nACSF (as described previously) supplemented with (in μM): 1 TTX, 25 CPP, 50 picrotoxin, and 5 CGP 55845 to isolate AMPAR-mediated mEPSCs. Whole-cell voltage clamp recordings were then performed upon transfected neurons (found upon visual observation with fluorescence) held at -60 mV with an Axopatch 400 amplifier (Molecular Devices, Sunnyvale, CA, USA) at room temperature (23-25 °C). Borosilicate patch pipettes (4-7 M $\Omega$ ) were filled with (in mM): 120 K-gluconate, 1 EGTA, 10 HEPES, 5 MgATP, 0.5 Na<sub>2</sub>GTP, 5 NaCl, 5 KCl, and 10 phosphocreatine K2 (pH7.2-7.3 with KOH and 285-295 mOsm). To monitor access resistance, transient test pulses were applied consistently every 2 min throughout the duration of the recording. Access resistance typically fell within the range of 7–10 G $\Omega$ , and data was discarded if the access resistance deviated > 20% during the recording. After holding current was stabilized, data was acquired at a sampling frequency of 20 kHz and filtered at 2 kHz for 10 min. All AMPAR-mEPSCs were identified offline through use of Mini Analysis Software (Synaptosoft, Decature, GA, USA). Thresholding for mEPSC amplitude detection was set at eight time the root-mean-square value of a visually-determined event-free recording span, and 300-450 events per cell were analyzed and utilized to determine mean values.

#### 2.7. Pharmacological treatments

To assess the effects of leupeptin, bafilomycin, and MG132 treatment upon spine density and NHE6 levels in transfected primary hippocampal neurons, leupeptin (100 µg/ml), bafilomycin A1 (100 nM), or MG132 (40 µM) were added to the culture media 24 h post-transfection, and cultures were left for an additional 24 h prior to fixation. In evaluating the effects of leupeptin upon the response to gly-ChemLTP, transfected neurons were pre-treated with either of these inhibitors in for  $\geq 30\, min$  prior to gly-ChemLTP stimulation and further processing.

#### 2.8. Confocal microscopy

Fixed and mounted primary neuron cultures were examined using a Leica SP2 confocal microscope with images acquired using  $40\times$  and

 $63 \times$  HCXPL APO oil-immersion objectives (NAs 1.25 and 1.4, respectively). GFP was imaged using a 488 nm Ar laser line, mCherry and PI were imaged using a 543 nm HeNe laser line, and Alexa Fluor 633 and 647 and Dylight 649 were imaged using a 633 nm HeNe laser line. Channels were acquired sequentially to prevent spectral overlap of fluorophores. Optical sections of 300–500 nm were taken and frame averaged  $3 \times$  at low resolution or line-averaged  $2 \times$  at high resolution to improve the signal-to-noise ratio. Live imaging of spine dynamics was performed using the same Leica SP2 confocal microscope with a  $63 \times$  water immersion long working distance lens (HXC APO L U-V-I; NA 0.9).

#### 2.9. Measurements and quantifications

All image stacks were first deconvolved using Huygens Essential software by using a full maximum likelihood extrapolation algorithm (Scientific Volume Imaging, Hilversum, The Netherlands), and 3D images and 4D time-lapse stacks were compiled as maximum intensity projections using the Surpass function on Imaris software (Bitplane AG, Zurich, Switzerland). Spines were then quantified using a detection/ classification program that automatically detected the length of the spine head and neck. From the ratio of the diameter and length of the head and neck of spines, it was possible to visually distinguish between stubby, mushroom, and long thin spines, as well as filopodia, based off of previously distinguished criteria (Harris et al., 1992; Sorra and Harris, 2000). In brief, if the spine had no visible distinction between its head and neck subregions, it was classified as stubby. If the spine was short had a larger head (>  $1 \, \mu m$  in diameter) and neck subregions, it was identified as mushroom. If it had a small head ( $< 1 \mu m$  in diameter) and was longer in length, it was counted as a long thin-type spine. Filopodia, precursors of either new dendrites or spines, were typically identified if they had 1) no distinguishable spine head and 2) a length of longer than 3 µm and were quantified separately. Colocalization analyses between transfected mCherry-tagged NHE6 WT and ΔES and EEA1, Stx-13, AF-Tfn, Rab7, LAMP1, and GluA1 were determined using the ImarisColoc algorithm, which generated a new channel (coloc) containing voxels representing channel overlap based off of a threshold of colocalization. Thresholds were applied consistently between images in order to remove subjectivity during the analysis. During these colocalization steps, the stacks were masked according to the dendritic EGFP signal to ensure that the puncta in question were indeed in the neuron itself. A puncta of individual or colocalized markers was counted as being localized to a dendritic spine if it was within  $\leq 0.5 \,\mu m$ of the spine. The proportion of spines containing single or colocalized markers in each image was then quantified. Next, protein localization within the spine was localized to its base (a), neck (b), or head (c), as previously described (Deane et al., 2013). The fraction of puncta in each spine subregion relative to the total number of puncta localized to spines was then determined.

For live imaging experiments, changes in the localization of mCherry-tagged NHE6 puncta were quantified in a similar fashion. Changes in spine head volume were also assessed as averages of spine head volume before and after gly-ChemLTP, as previously described (Chang et al., 2014). Briefly, the time-lapse confocal image stacks were four-dimensionally rendered using the Surpass function of Imaris. The spines of interest were then isolated at each time point, and the volume was automatically calculated. In this case, volume changes in all thin and mushroom spines in response to gly-ChemLTP were measured relative to their baseline values. However, stubby spines were excluded because the resolution limit of light microscopy prevents their proper volume analysis. The distribution and number of spine subtypes were also quantified before and after gly-ChemLTP, and the changes in their number were calculated relative to baseline values.

#### 2.10. Statistical analyses

The data represent the mean  $\pm$  the standard error of the mean (S.E.M.) and statistical analyses were performed using the Student's t-test, Dunn's multiple comparison test, or a one-way analysis of variance (ANOVA) followed by a Bonferroni post-hoc test. A minimum p-value of < 0.05 was considered significant.

#### 3. Results

#### 3.1. NHE6 ΔES reduces excitatory synaptic density

To assess the impact of the  $\Delta ES$  mutant on neuronal morphology and function in vitro, we used primary hippocampal neuron cultures prepared from early postnatal C57BL/6 mice as previously described (Brewer and Torricelli, 2007). At 10-12 days in vitro (DIV), the cultures were co-transfected with DNA plasmids encoding enhanced green fluorescent protein (EGFP) to demarcate neuronal morphology and either mCherry fluorescent protein (mCh) (as a co-transfection control), mCh-tagged WT NHE6 (NHE6<sub>WT</sub>-mCh) or the  $\Delta$ ES mutant (NHE6<sub> $\Delta$ ES</sub>mCh). Although neurons express endogenous WT NHE6, we posit that the  $\Delta$ ES mutant exerts a dominant-negative effect in this culture system based on the following observations. Firstly, we showed previously that the transfected  $\Delta$ ES mutant can physically interact with WT NHE6, as observed through co-immunoprecipitation experiments performed on HeLa cells. Secondly, we also demonstrated that fluorescently-tagged NHE6 WT and  $\Delta$ ES constructs strongly colocalize with WT NHE6 when expressed in Chinese hamster ovary AP-1 cells, further suggesting that the  $\Delta ES$  mutant is capable of forming heterodimers with WT NHE6(Ilie et al., 2016). Thirdly, in the present study, we found that NHE6 $_{\Delta ES}$ -mCh transfection attenuated the trafficking of total NHE6 (i.e., endogenous WT plus exogenous  $\Delta$ ES, as measured by immunostaining with a rabbit polyclonal NHE6 antibody capable of recognizing both WT and ΔES NHE6) into spines located on the distal dendrites of primary hippocampal neurons (Fig. S1; Table S1). Overall, the data imply that exogenous ΔES NHE6 heterodimerizes with endogenous WT NHE6 and impairs its trafficking into dendrites, presumably diminishing overall NHE6 function at excitatory postsynaptic sites in transfected cells as a

In the current study, we extend our analysis of the  $\Delta ES$  mutant by examining whether changes in dendritic arbor are accompanied by changes in excitatory synaptic structure. As shown in Fig. 1A, B and Table S2, secondary and tertiary dendrites of primary hippocampal neurons transfected with NHE6 $_{\Delta ES}$ -mCh showed a significant decrease in overall spine density, with significant reductions in both mushroom-and thin-type dendritic spines when compared to the mCh control or NHE6 $_{WT}$ -mCh. Concurrent with this decrease in spines, we also observed a reciprocal increase in the density of filopodia, immature structures that may develop into either new spines or dendritic branches (Koleske, 2013), in NHE6 $_{\Delta ES}$ -mCh transfected cells (Fig. 1A, C; Table S2). Overall, these data indicate that introducing NHE6 $_{\Delta ES}$ -mCh into primary hippocampal neurons has a deleterious effect on the maintenance of spine density and morphology.

#### 3.2. Differential intracellular localization of NHE6 WT and $\Delta$ ES

Next, we investigated if there was a difference in the neuronal subcellular localization of  $\rm NHE6_{\Delta ES}$ -mCh compared to  $\rm NHE6_{WT}$ -mCh. We found that in dendrites,  $\rm NHE6_{WT}$ -mCh localized to approximately 75% of dendritic spines, with the majority present in the base and head subregions. In contrast,  $\rm NHE6_{\Delta ES}$ -mCh was present in only 40% of spines and localized mainly to the spine base, with significantly less present in the spine head (Fig. 1A, D–E; Table S2). This suggests that the trafficking of  $\rm NHE6_{\Delta ES}$ -mCh to excitatory synaptic sites may be compromised.

In most cell types, internalized plasma membrane cargo is initially

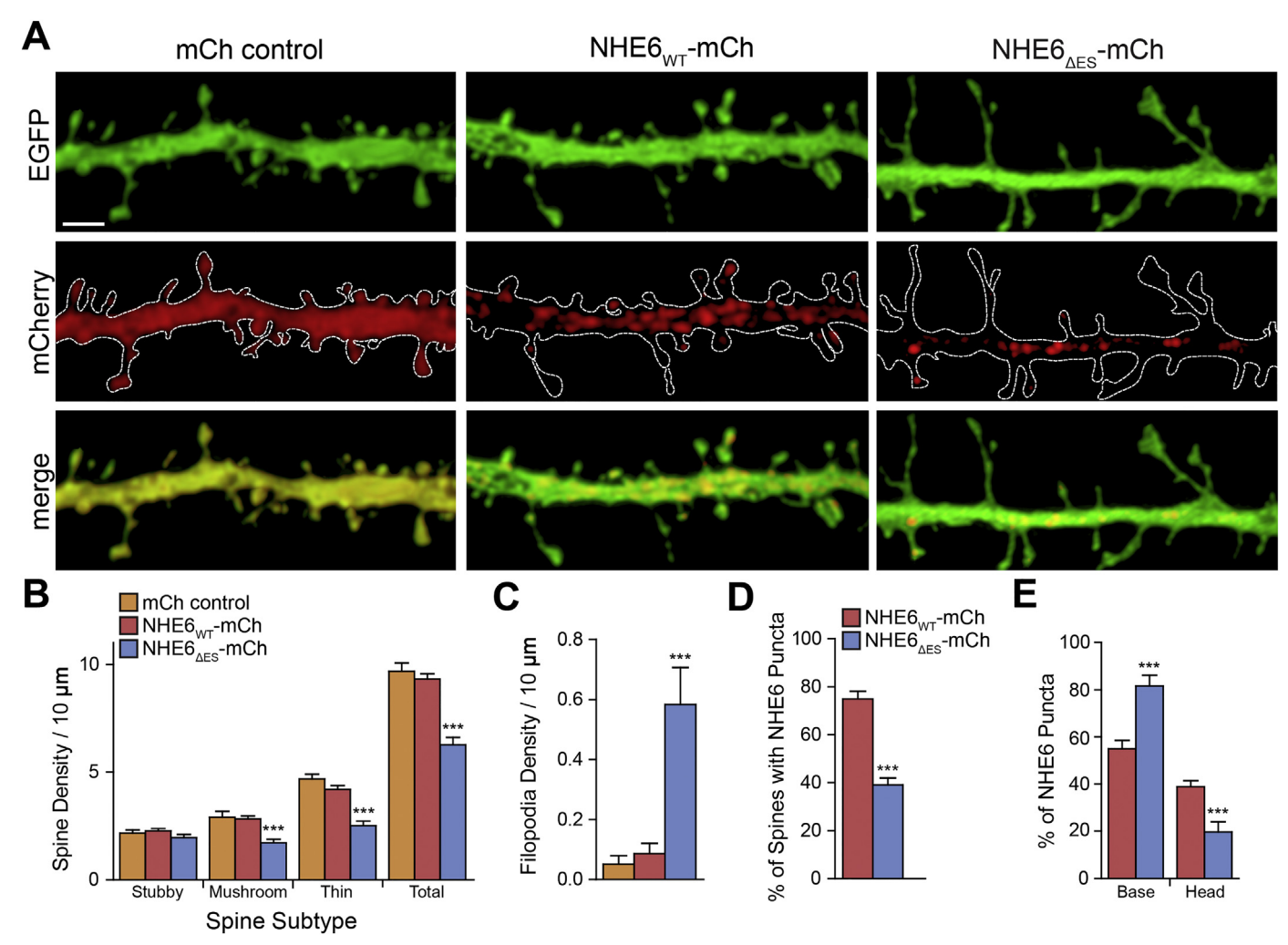


**Fig. 1.** NHE6 ΔES overexpression reduces the density of mature dendritic spines in hippocampal pyramidal neurons. A: Representative confocal images of primary hippocampal neurons transfected with EGFP and mCh alone (as a transfection control), NHE6<sub>WT</sub>-mCh, or NHE6<sub>ΔES</sub>-mCh. EGFP and mCh channels are shown individually and merged; white outlines denote location of EGFP-positive dendrite. Scale bar:  $2 \mu m$ . B–C: Mean  $\pm$  S.E.M. density of all and each major spine subtype, i.e. stubby, mushroom, and thin (B), as well as filopodia (C). D: Mean  $\pm$  S.E.M. fraction of spines containing puncta of transfected, overexpressed NHE6 WT or ΔES puncta of all spines analyzed for each transfection condition. E: Mean  $\pm$  S.E.M proportion of spine-localized puncta of overexpressed NHE6 WT and ΔES in the base and head subregions of spines. mCh control: n = 543 spines and 3 filopodia along 560.636 μm of dendrite from 20 cells; NHE6 WT: n = 549 spines and 4 filopodia along 591.383 μm of dendrite from 20 cells; NHE6 ΔES: n = 360 spines and 34 filopodia along 577.992 μm of dendrite from 20 cells, 6 separate experiments. For NHE6 puncta counts, NHE6 WT: n = 1940 spines along 2615.825 μm of dendrite from 90 cells; NHE6 ΔES: n = 1292 spines and 2600.605 μm of dendrite from 90 cells, 29 separate experiments. \*\*p < .01; \*\*\*p < .001; Dunnett's Multiple Comparison Test (B-C); independent Student's t-test, two-tailed (D-E).

sorted to early endosomes, where it may be trafficked either back to the cell surface via recycling endosomes for reuse or redirected to lysosomes for degradation (illustrated in Fig. 2D) (Grant and Donaldson, 2009; Maxfield and McGraw, 2004). In a previous study in neurons (Deane et al., 2013), we reported that endogenous NHE6 colocalizes with early endosomal antigen-1 (EEA1), an early endosome marker (Mu et al., 1995), as well as syntaxin-12/13 (stx-13) and AlexaFluor 633-Transferrin (AF-Tfn), both markers for recycling endosomes (Prekeris et al., 1998; Willingham et al., 1984). We assessed whether the localization of the  $\Delta ES$  mutant with these endosomal markers is altered in spines and further calculated the degree of colocalization using thresholded Mander's coefficients. We found that NHE6 $_{\Delta ES}$ -mCh showed a significant reduction in colocalization with EEA1, stx-13, and AF-Tfn in comparison to NHE6WT-mCh (Fig. 2; Table S3). Interestingly, levels of AF-Tfn, which is internalized in a clathrin/adaptor protein 2 (AP2)dependent process, were downregulated in the dendrites of  $\Delta ES$ -positive cells (Fig. 2C, E; Table S3), corroborating our previous observations in AP-1 and HeLa cells, and neuronal soma (Ilie et al., 2016). Together, these results suggest the  $\Delta ES$  mutant is mislocalized and alters trafficking of at least some endocytosed cargo.

We have previously demonstrated in live non-neuronal AP-1 cells that NHE6  $\Delta$ ES-containing endosomes are more acidic than those containing NHE6 WT (Ilie et al., 2016). Hence, we further probed the subcellular localization of the ΔES mutant using markers of acidic organellar compartments of the degradative pathway (Mellman et al., 1986). To this end, we performed immunostaining for Rab7, a marker for late endosomes/multivesicular bodies (Vanlandingham and Ceresa, 2009), as well as lysosomal-associated membrane protein 1 (LAMP1), a lysosomal marker (Carlsson and Fukuda, 1989). As shown visually (Fig. 3A-B) and quantitatively (Fig. 3D-F; Table S4), colocalization with Rab7 and LAMP1 was greater in NHE6 $_{\Delta ES}$ -mCh compared to WT. In addition, we found a significant increase in LAMP1 puncta at spines in NHE6 $_{\Delta ES}$ -mCh-transfected cells (Fig. 3B–C; Table S4), indicating an increase of lysosomal bodies in these neurons. Overall, the data suggest that  $\Delta ES$  mutant vesicles are directed away from early and recycling endosomes toward late endosomes and lysosomes.

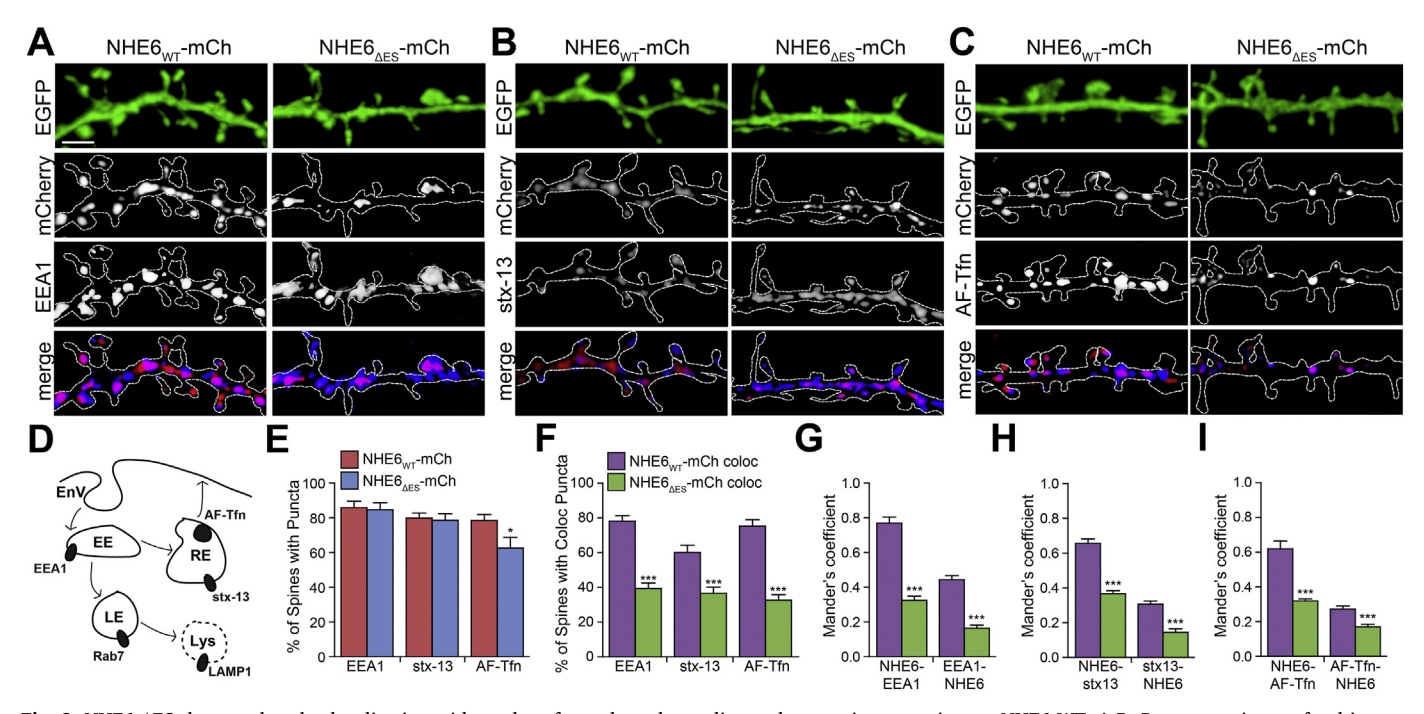


Fig. 2. NHE6 ΔES shows reduced colocalization with markers for early and recycling endosomes in comparison to NHE6 WT. A-D: Representative confocal images showing a section of secondary or tertiary dendrite of a primary hippocampal neuron co-transfected with EGFP and NHE6<sub>WT</sub>-mCh or NHE6<sub>ΔES</sub>-mCh and immunolabeled with an early endosomal marker, early endosomal antigen 1 (EEA1, A) or recycling endosomal markers syntaxin 12/13 (stx-13, B) and AlexaFluor633-Transferrin (AF-Tfn, C). Channels are shown separately and merged; white outlines denote location of EGFP-positive dendrite. Scale bar: 2 μm. D: Representative schematic of different endolysosomal compartments within the cell, with the utilized markers for each major compartment. EnV: endocytic vesicle; EE: early endosome; RE: recycling endosome; LE: late endosome, Lys: lysosome. E: Mean ± S.E.M. fraction of spines containing puncta of EEA1, stx-13, and AF-Tfn of all spines analyzed for each transfection condition. F: Quantification of the mean ± S.E.M. fraction of spines containing colocalized puncta of overexpressed NHE6 WT or ΔES and each vesicular marker of all spines analyzed. G-I: Mean ± S.E.M. thresholded Mander's coefficient values between NHE6 WT or ΔES and EEA1 (G), stx-13 (H), and AF-Tfn (I). For EEA1, NHE6 WT: n = 242 spines along 293.30 μm of dendrite from 10 cells; NHE6 ΔES: n = 135 spines along 296.81 μm of dendrite from 10 cells, 3 separate experiments. For stx-13, NHE6 WT: n = 148 spines along 295.97 μm of dendrite from 10 cells; NHE6 ΔES: n = 116 spines from 309.07 μm of dendrite from 10 cells, 4 separate experiments. For AF-Trf, NHE6 WT: n = 148 spines along 295.97 μm of dendrite from 10 cells; NHE6 ΔES: n = 116 spines from 309.07 μm of dendrite from 10 cells, 4 separate experiments. For AF-Trf, NHE6 WT: n = 148 spines along 295.97 μm of dendrite from 10 cells; NHE6 ΔES: n = 116 spines from 309.07 μm of dendrite from 10 cells, 4 separate experiments.

#### 3.3. NHE6 $\Delta$ ES disrupts AMPA receptor trafficking

Next, we looked for signs of dysregulation of synaptic cargo in NHE6<sub>AES</sub>-mCh cells by assessing the localization of glutamatergic AMPARs, which mediate most fast excitatory neurotransmission in the central nervous system (McKinney, 2010). We have already shown that endogenous WT NHE6 colocalizes strongly with the GluA1 subunit of AMPARs (Deane et al., 2013), and we have recapitulated that finding in transfected NHE6<sub>WT</sub>-mCh neurons (Fig. 4A-C; Table S5). However, this overlap was significantly attenuated in neurons expressing NHE6 $_{\Delta ES}$ mCh and was accompanied by a significant decrease in GluA1 puncta at spines (Fig. 4A–C; Table S5), indicating that the  $\Delta$ ES mutant also deters the trafficking of GluA1 to excitatory synapses. To investigate if this decrease in GluA1 levels was due to enhanced trafficking of these receptors to lysosomes in the presence of the  $\Delta$ ES mutant, we co-transfected neurons with EGFP and influenza virus hemagglutinin (HA)tagged constructs of NHE6 WT or  $\Delta$ ES to allow for double immunolabeling of the lysosomal marker LAMP1 and GluA1. Interestingly, in NHE6 $_{AES}$ -HA-expressing cells, there was greater colocalization between LAMP1 and GluA1 compared to neurons expressing NHE6WT-HA (Fig. 4D-F; Table S5). This finding implies that in the presence of the ΔES mutant, GluA1 is preferentially targeted to lysosomal compartments rather than recycling endosomes, which may result in their enhanced degradation.

#### 3.4. NHE6 $\Delta$ ES impairs the response to glycine-mediated chemical LTP

Enhanced delivery of AMPARs to the post-synaptic compartment is an important contributing factor for generating long-term potentiation (LTP), a cellular model of learning and memory (Lynch, 2004; Malenka and Nicoll, 1999; Park et al., 2004; Petrini et al., 2009). Given that NHE6 is implicated in the trafficking of AMPARs, we assessed whether the  $\Delta$ ES mutation also impairs the response to LTP in hippocampal neurons. To investigate the insertion of GluA1-containing AMPARs into synaptic sites following LTP (Selcher et al., 2012), we initially cotransfected neurons with tdTomato (tdT) and N-terminal fused pHsensitive superecliptic pHluorin (SEP)-GluA1 (sGluA1) alone, or with HA-tagged NHE6 WT or  $\Delta$ ES. We then subjected live transfected cells to a glycine-mediated chemical LTP (gly-ChemLTP) protocol to emulate NMDA receptor (NMDAR)-dependent LTP induction at Schaffer collateral-CA1 synapses in the hippocampus (Deane et al., 2013; Fortin et al., 2010). If LTP is functioning properly, we would expect to see an increase in sGluA1 fluorescence in spine heads. Twenty minutes following gly-ChemLTP induction in tdT control- and NHE6<sub>WT</sub>-HA-transfected neurons, we observed a significant increase in the number of spines containing sGluA1 and an upregulation of their puncta in the heads of these spines compared to unstimulated sister control cultures (Fig. 5A-C; Table S6). In contrast, gly-ChemLTP stimulation in NHE6<sub>AES</sub>-HA-expressing neurons did not show an increase in sGluA1 localization at spines or within the spine head compared to unstimulated controls (Fig. 5A-C; Table S6). To verify the NMDAR dependency of this protocol, additional sister NHE6<sub>WT</sub>-HA-expressing cultures were subjected to gly-ChemLTP supplemented with (RS)-3-(2carboxypiperazin-4-yl)-propyl-1-phosphonic acid ((RS)-CPP), a potent NMDAR antagonist (Davies et al., 1986). As expected, these cells did not show an upregulation of sGluA1 puncta at spines or in spine heads (Fig. S2A-C; Table S7). Hence, in addition to preventing GluA1 trafficking to spines, NHE6 $_{\Delta ES}$ -HA impairs the insertion of AMPARs at the

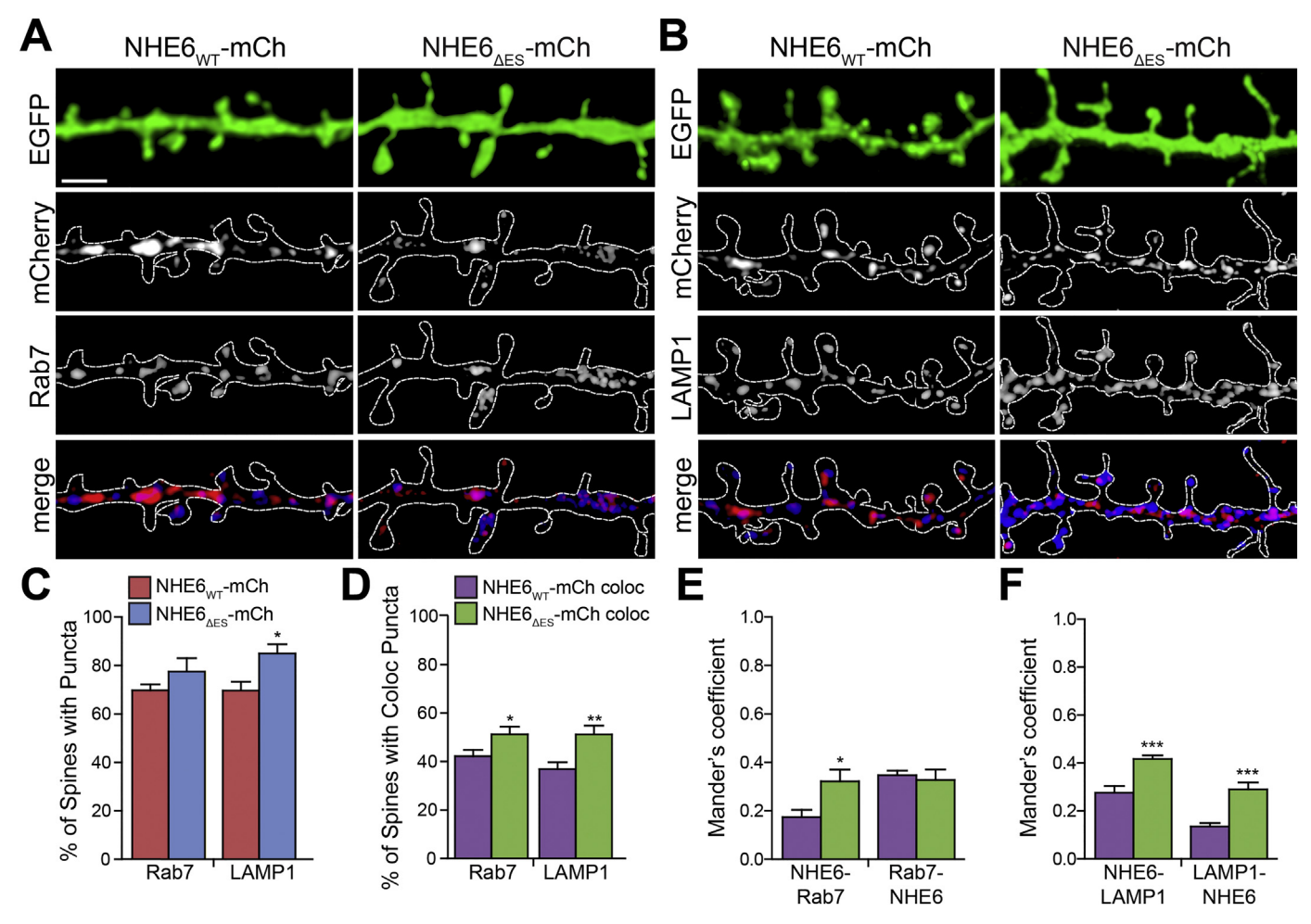


Fig. 3. In contrast to NHE6 WT, NHE6 ΔES shows increased colocalization with markers for late endosomes and lysosomes, more acidic compartments. A-B: Representative confocal images showing a section of secondary or tertiary dendrite of a primary hippocampal neuron co-transfected with EGFP and NHE6<sub>WT</sub>-mCh or NHE6<sub>ΔES</sub>-mCh and immunolabeled with the late endosomal marker Ras-related protein Rab7 (A) or the lysosomal marker lysosomal associated membrane protein 1 LAMP1 (B). Channels are shown separately and merged; white outlines denote location of EGFP-positive dendrites. Scale bar:  $2 \,\mu m$ . C: Quantification of the mean  $\pm$  S.E.M. fraction of spines containing puncta of Rab7 or LAMP1 of all spines analyzed under each transfection condition. D: Quantification of the mean  $\pm$  S.E.M. fraction of spines containing colocalized puncta of overexpressed NHE6 WT or ΔES and Rab7 or LAMP1 of all spines analyzed. *E-F*: Quantified mean  $\pm$  S.E.M. thresholded Mander's coefficient values between NHE6 WT or ΔES and Rab7 (E) or LAMP1 (F). For Rab7, NHE6 WT: n = 210 spines along 232.69 μm of dendrite from 8 cells; NHE6 ΔES: n = 176 spines from 235.88 μm of dendrite from 8 cells, 3 separate experiments. For LAMP1, NHE6 WT: n = 212 spines along 289.24 μm of dendrite from 10 cells; NHE6 ΔES: n = 132 spines from 269.44 μm of dendrite from 10 cells, 4 separate experiments. \*p < .05; \*\*p < .01, \*\*\*p < .001, independent Student's t-test, two-tailed for all other comparisons.

#### cell surface following NMDAR-dependent LTP.

Does this impairment in AMPAR trafficking lead to functional changes in synaptic strengthening? To address this, we acquired wholecell voltage clamp recordings of AMPAR-mediated miniature excitatory postsynaptic currents (mEPSCs) from transfected hippocampal cells 20 min after gly-ChemLTP induction. Normally, cells subjected to LTP stimulation show an increase in mEPSC amplitude compared to unstimulated sister cultures due to the addition of AMPARs at the cell surface (Chater and Goda, 2014). Accordingly, we found that gly-ChemLTP-stimulated mCh- and NHE6WT-mCh-expressing cells showed an increase in overall mEPSC amplitude compared to untreated sister cultures. In contrast, stimulated NHE6  $_{\Delta ES}\text{-}m\text{Ch-expressing}$  cells failed to show a significant increase in mEPSC amplitude (Fig. 5D-E; Table S6). Again, this increase in mEPSC amplitude in NHE6WT-mCh-expressing cells was NMDAR-dependent, as we observed no change in mEPSC amplitude in additional NHE6<sub>WT</sub>-mCh-transfected cultures subjected to gly-ChemLTP in the presence of (RS)-CPP (Fig. S2D-E; Table S7). Given the large variation in inter-event intervals between dissociated culture preparations, we did not assess mEPSC frequency using this method. Significant differences were not observed in other mEPSC parameters

(e.g. rise and decay times) across conditions. Overall, these findings demonstrate that the  $\Delta ES$  mutant impairs excitatory synaptic potentiation in response to gly-ChemLTP.

Functional potentiation is normally accompanied by structural changes at the synapse, including an increase in spine head volume (SHV) as well as the potential formation of new spines (Forrest et al., 2018; Fortin et al., 2010; Park et al., 2006; Sorra and Harris, 2000). We previously reported that endogenous NHE6 is recruited to the heads of dendritic spines following gly-ChemLTP stimulation (Deane et al., 2013). Now, we investigated whether the recruitment of exogenous NHE6 also occurs in response to gly-ChemLTP in transfected neurons. We performed time-lapse confocal imaging on a section of dendrite for 15 min to establish a structural baseline, stimulated for 10 min, and then continued to image for an additional 20 min (Fig. 6B). Following gly-ChemLTP stimulation, NHE6WT-mCh-expressing neurons exhibited a significant increase in the percentage of NHE6-containing spines, with NHE6 puncta being redistributed from the base to the heads of these spines. In contrast, NHE6  $_{\Delta ES}\text{-mCh}$  puncta did not traffic to spines. Moreover, mushroom- and thin-type spines on NHE6 $_{\Delta ES}$ -mCh-transfected neurons failed to show significant enlargements of SHV

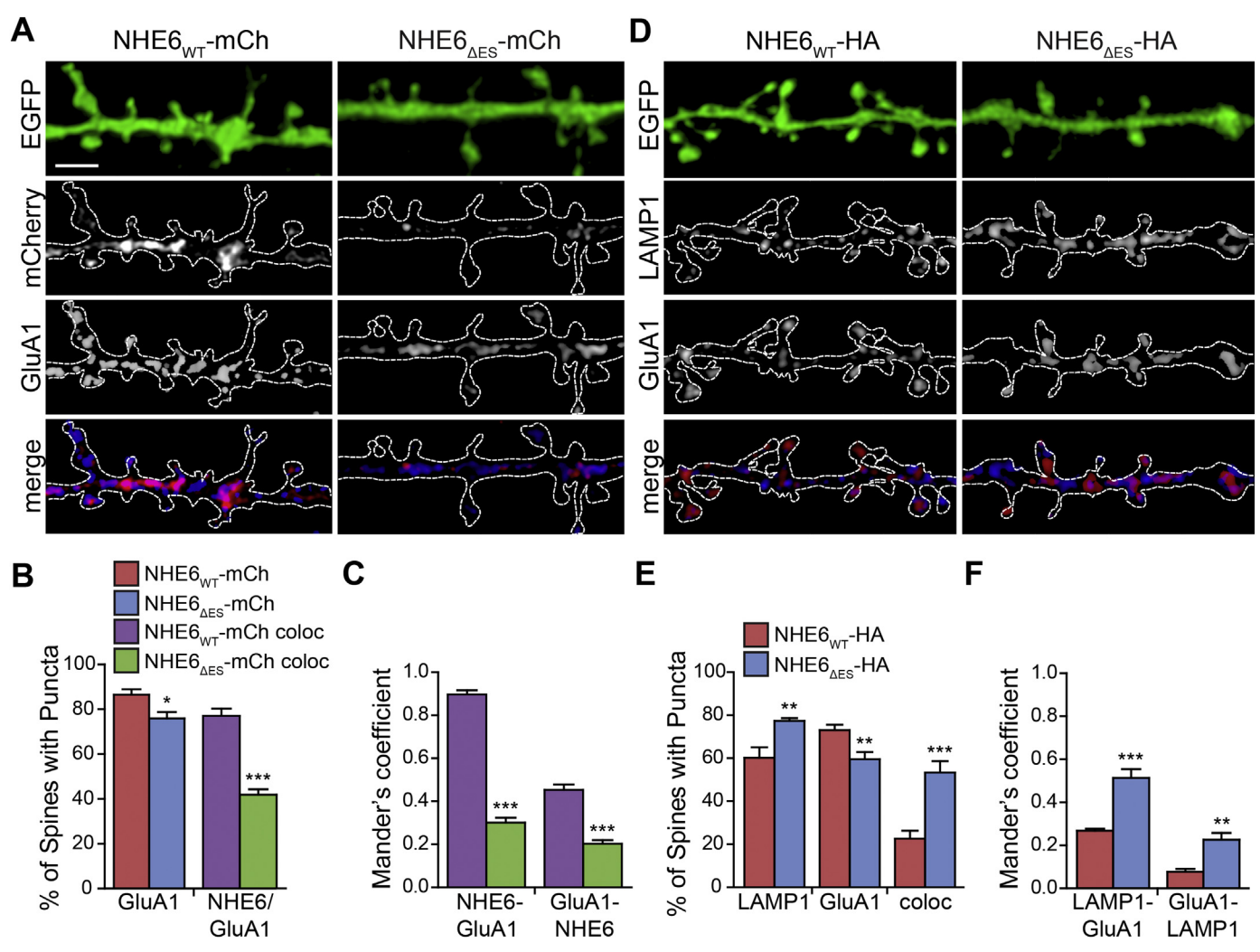


Fig. 4. NHE6 ΔES transfection attenuates the trafficking of GluA1-containing AMPA receptors to spines and enhances their localization to lysosomes. At Representative confocal images showing a section of the secondary or tertiary dendrite of a primary hippocampal neuron co-transfected with EGFP and NHE6<sub>MT</sub>-mCh or NHE6<sub>ΔES</sub>-mCh and immunolabeled for the AMPA receptor subunit GluA1. Channels are shown separately and merged; white outlines denote location of EGFP-positive dendrite. Scale bar:  $2 \, \mu m$ . B: Mean  $\pm$  S.E.M. fraction of spines containing puncta of GluA1 (left) or colocalized puncta of NHE6 and GluA1 (right) of all spines analyzed under each transfection condition. C: Mean  $\pm$  S.E.M. thresholded Mander's coefficient values between NHE6 WT or ΔES and GluA1. D: Representative confocal images showing a section of the secondary or tertiary dendrite of a primary hippocampal neuron co-transfected with EGFP and NHE6<sub>WT</sub>-HA or NHE6<sub>ΔES</sub>-HA and double immunolabeled for GluA1 and LAMP1. E: Quantification of the mean  $\pm$  S.E.M. fraction of spines containing puncta of LAMP1 (left), GluA1 (center), and colocalized puncta of LAMP1 and GluA1 (right) of all spines analyzed under each transfection condition. F: Quantified mean  $\pm$  S.E.M. thresholded Mander's coefficient values between LAMP1 and GluA1 under each transfection condition. For GluA1, NHE6 WT: n = 190 spines along 288.93 μm of dendrite from 10 cells; NHE6 ΔES: n = 129 spines along 281.50 μm of dendrite from 10 cells; NHE6 WT: n = 182 spines along 152.725 μm of dendrite from 6 cells; NHE6 ΔES: n = 116 spines along 151.752 μm of dendrite from 6 cells, NHE6 ΔES: n = 116 spines along 151.752 μm of dendrite from 6 cells, NHE6 ΔES: n = 116 spines along 151.752 μm of dendrite from 6 cells, NHE6 ΔES: n = 116 spines along 151.752 μm of dendrite from 6 cells, NHE6 ΔES: n = 116 spines along 151.752 μm of dendrite from 6 cells, NHE6 ΔES: n = 116 spines along 151.752 μm of dendrite from 6 cells, NHE6 ΔES: n = 116 spines along 151.752 μm of dendrite

compared to controls in response to gly-ChemLTP (Fig. 6A, C–H; Table S8). As such, mCh- and NHE6 $_{\rm WT}$ -mCh-expressing neurons showed a more significant change from baseline in SHV across spine subtypes when compared to NHE6 $_{\rm AES}$ -mCh-transfected neurons (Fig. 6I; Table S8). These changes in NHE6 recruitment and SHV in NHE6 $_{\rm WT}$ -mCh-transfected neurons were also blocked by (RS)-CPP included in the gly-ChemLTP stimulation solution, again demonstrating NMDAR dependency (Fig. S2F–I; Table S7). Together, the data demonstrate that the  $_{\rm AES}$  mutant disrupts both the functional and morphological response to gly-ChemLTP induction by impairing recycling endosomal trafficking within the dendrites of hippocampal neurons.

## 3.5. Restoring spine density and remodeling in NHE6 $\Delta$ ES-expressing neurons

Next, we explored whether it was possible to restore these deficits in

neuronal morphology, receptor trafficking and plasticity in ΔES-expressing neurons. As noted previously, the  $\Delta$ ES mutant induces excess acidification (Ilie et al., 2016) and an increase in spine-localized endolysosomal vesicles (Fig. 3). Considering these results, we sought to prevent potential endolysosomal degradation by treating cultures (24 h post-transfection) overnight with leupeptin (100 µg/ml), a reversible, competitive antagonist of endolysosomal proteases, or bafilomycin A1 (100 nM), a vacuolar H<sup>+</sup>-ATPase inhibitor. Compared to untreated  $NHE6_{\Delta ES}$ -mCh-expressing neurons, we found that leupeptin treatment restored the densities of all three spine types (stubby, thin and mushroom) to levels comparable with the spine densities of untreated mChor NHE6<sub>WT</sub>-mCh-transfected neurons (Fig. 7A-E; Table S9). By comparison, bafilomycin appeared to partially restore only the density of thin spines compared to untreated NHE6  $_{\Delta ES}\text{-}m\textsc{Ch-expressing}$  neurons cultures. On the other hand, mCh- and NHE6WT-mCh-expressing neurons were not profoundly affected by treatment with leupeptin.

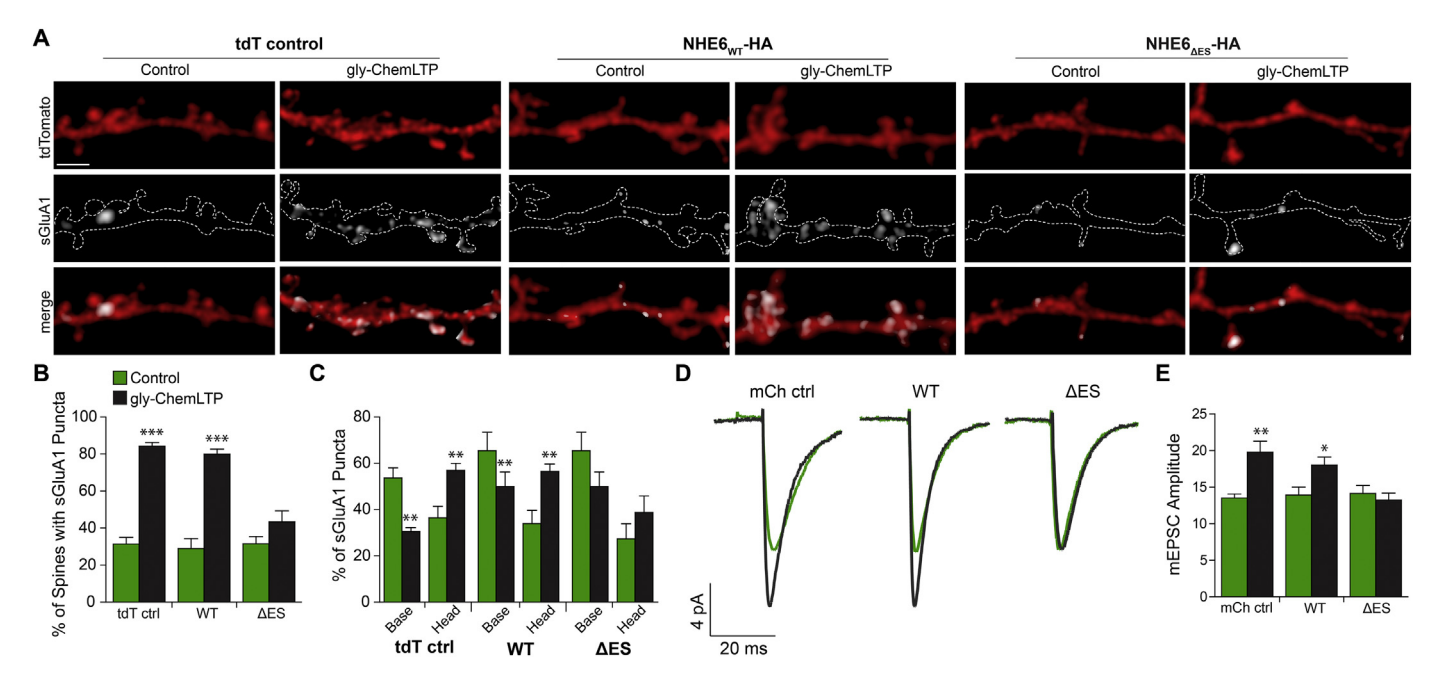


Fig. 5. NHE6 ΔES-expressing cells fail to show insertion of GluA1-positive AMPA receptors at spines and potentiation of miniature excitatory postsynaptic current (mEPSC) amplitude following glycine-mediated chemical LTP. A: Representative confocal micrographs of secondary or tertiary dendrites from transfected primary hippocampal neurons for sister unstimulated control and gly-ChemLTP-stimulated cultures for each transfection condition. Channels are shown separately and merged; white outlines denote location of tdTomato-positive dendrite. Scale bar:  $2 \mu m$ . B: Mean  $\pm$  S.E.M. percentage of spines containing surface SEP-GluA1 (sGluA1) puncta for control and glyChemLTP conditions for each transfection condition. C: Mean  $\pm$  S.E.M. proportion of sGluA1 puncta in each spine subregion for control, gly-ChemLTP-stimulated, and CPP-treated, gly-ChemLTP-stimulated cultures. For tdT control: n = 125 spines along 188.156 μm of dendrite from 8 cells; gly-ChemLTP: n = 150 spines along 197.145 μm of dendrite from 8 cells; for NHE6 WT, control: n = 100 spines along 156.529 μm of dendrite from 8 cells, gly-ChemLTP: n = 116 spines along 191.817 μm of dendrite from 8 cells; for NHE6 ΔES, control: n = 100 spines along 191.817 μm of dendrite from 8 cells; for NHE6 ΔES, control: n = 100 spines along 192.52 μm of dendrite from 8 cells, gly-ChemLTP: n = 116 spines along 193.374 μm of dendrite from 8 cells. D: Average AMPAR-mEPSC event trace of an unstimulated control and gly-ChemLTP-stimulated cell for each transfection condition. E: Mean  $\pm$  S.E.M. mEPSC amplitude of all cells analyzed under each stimulation and transfection conditions. For all conditions, n = 14 cells, 5 separate experiments. n = 100 spines along 193.374 μm of dendrite from 8 cells: n = 100 spines along 193.374 μm of dendrite from 8 cells: n = 100 spines along 193.374 μm of dendrite from 8 cells: n = 100 spines along 193.374 μm of dendrite from 8 cells: n = 100 spines along 193.374 μm of dendrite from 8 cells: n = 100 spines along 194

Moreover, bafilomycin administration significantly reduced the density of each spine subtype as well as total spine density (Fig. 7A-E; Table S9). When we quantified NHE6 levels following these treatments, we found overall levels of NHE6wr-mCh were not significantly changed relative to control (Fig. 7A, F; Table S9). However, leupeptin and bafilomycin significantly increased the fraction of spines containing NHE6<sub>AES</sub>-mCh puncta compared to untreated controls (Fig. 7A, F; Table S9). As we previously reported that the  $\Delta$ ES mutant is also subjected to partial degradation by the proteasome (Ilie et al., 2016), we investigated whether inhibition of the proteasome could restore spine density. However, application of the general proteasomal inhibitor MG132 (40 μM) did not increase spine density in NHE6<sub>ΔES</sub>-mCh-expressing neurons, nor did it significantly increase NHE6 AES-mCh trafficking to spines (Fig. 7; Table S9). Collectively, these data show that specifically preventing lysosomal degradation mitigates some of the morphological deficits induced by expression of the  $\Delta ES$  mutant.

Based on the above findings, we next examined whether the defective functional and structural response to LTP in NHE6\_{\Delta ES}-mCh-transfected cells could be restored by acutely pre-treating transfected cultures with leupeptin (100 µg/ml) for 30 min prior to the gly-ChemLTP protocol. It has previously been shown that 30 min of leupeptin treatment can enhance activated levels of the neurotrophic TrkB receptor in NHE6 KO neurons (Ouyang et al., 2013), indicating that this time frame is sufficient to prohibit aberrant endolysosomal degradation and restore receptor trafficking. Twenty min post-stimulation, we again probed for the subcellular distribution of sGluA1 and found significant insertion of GluA1 into the cell surface in  $\Delta$ ES-expressing cells, similar to controls (Fig. 8A–C; Table S10). Whole-cell voltage clamp recordings revealed that pre-treatment with leupeptin did not significantly alter mEPSC amplitude in mCh- and NHE6\_WT-mCh-transfected cells or their ability to potentiate beyond the stimulatory effects observed in the

absence of leupeptin (see Fig. 5D–E). In contrast, leupeptin-treated NHE6 $_{\Delta ES}$ -mCh–transfected neurons restored the increases in mEPSC amplitude following gly-ChemLTP stimulation comparable to levels in mCh- and NHE6 $_{WT}$ -mCh-transfected cells (compare Fig. 8D–E; Table S10 and Fig. 5E, Table S6).

Given that inhibiting excessive endolysosomal proteolysis helped restore the functional response to LTP, we performed additional timelapse confocal imaging experiments to assess the impact of leupeptin on spine structural remodeling after LTP. Following 30 min pre-treatment with leupeptin, NHE6<sub>AES</sub>-mCh-expressing cells showed both enhanced recruitment of NHE6<sub>ΔES</sub>-mCh puncta to spines, as well as an enlargement in thin-type spines comparable to controls in response to gly-Chem LTP stimulation (Fig. 9A-H; Table S11). Interestingly, leupeptintreated mCh- and NHE6<sub>WT</sub>-mCh-positive neurons did not show a significant increase in mushroom-type spines, though their relative increase in spine head volume was still greater than that of NHE6  $_{\Delta ES}\text{-mCh}$ transfectants (Fig. 9E-F, H; Table S11). Overall, these data strongly indicate an elevated accumulation of endolysosomal vesicles in the vicinity of spines in NHE6  $_{\Delta ES}\text{-mCh}$  transfectants. They also demonstrate that inhibiting endolysosomal mediated proteolysis restores the ability of ΔES-expressing neurons to structurally remodel and recruit AMPARs to the cell surface in response to gly-ChemLTP.

#### 4. Discussion

In recent years, studies on CS have expanded the genetic and phenotypic heterogeneity of this disorder (Garbern et al., 2010; Gilfillan et al., 2008; Pescosolido et al., 2014; Takahashi et al., 2011), yet the impact of these genetic alterations on cellular trafficking and learning mechanisms in neurons remains to be fully elucidated. In the present study, we chose to focus on the  $\Delta$ ES (p.E287\_S288del) mutation because

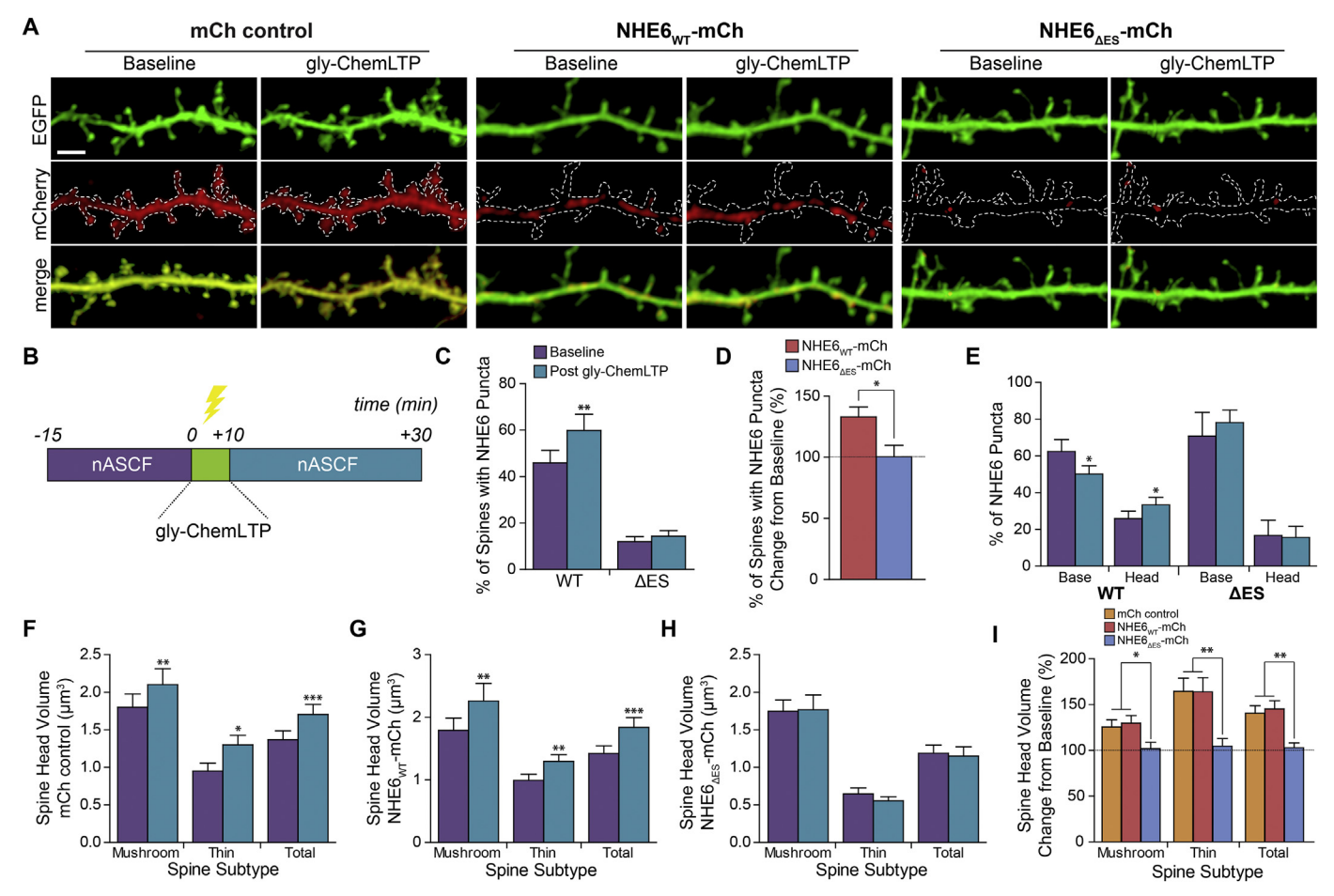


**Fig. 6.** NHE6 ΔES inhibits the structural response to gly-ChemLTP. A: Representative confocal micrographs of secondary or tertiary dendrites from transfected neurons at baseline and post gly-ChemLTP for each transfection condition. Channels are shown separately and merged; white outlines denote location of EGFP-positive dendrite. Scale bar: 3 μm. B: Schematic showing the time course of the gly-ChemLTP protocol. C: Mean  $\pm$  S.E.M. percentage of spines containing NHE6 WT or ΔES puncta at baseline and 20 min post gly-ChemLTP. D: Following gly-ChemLTP, the mean  $\pm$  S.E.M. percent change of NHE6 WT or ΔES-positive spines. E: Mean  $\pm$  S.E.M. proportion of NHE6 WT or ΔES puncta in each spine subregion at baseline and following gly-ChemLTP. F-H: Mean  $\pm$  S.E.M. spine head volume measurements for mushroom, thin, and total spines in mCh control- (F), NHE6 WT- (G), and NHE6 ΔES- (H)-transfected neurons at baseline and 20 min following gly-ChemLTP. I: Mean  $\pm$  S.E.M. percent change in spine head volume from baseline (100%) following gly-ChemLTP for each spine subtype under each transfection condition. mCh control: n = 173 spines along 206.597 μm of dendrite from 8 cells; NHE6 WT: n = 155 spines along 210.906 μm of dendrite from 4 cells, NHE6 ΔES: 142 spines along 210.201 μm of dendrite from 8 cells; 3 separate experiments.  $^*p < .05$ ,  $^**p < .01$ ,  $^{***}p < .0001$ ; paired Student's t-test, two-tailed (C-H), one-way ANOVA with Berforroni post-hoc test (I).

this was amongst the first SLC9A6 mutations to be reported that resulted in a largely intact protein (as opposed to other mutations that introduce a premature stop codon into the gene) (Gilfillan et al., 2008). In this particular study, the authors reported that all affected individuals included in the study showed profound developmental delay and learning problems. Furthermore, deletions of the analogous glutamate residue in other NHE family members, such as NHE1 and NHE8, has previously been shown to ablate ion transport function (Ding et al., 2006; Nakamura et al., 2005), and we have also reported that the  $\Delta ES$ mutation impaired the ability of NHE6 to regulate vesicular pH as well (Ilie et al., 2016). Thus, this mutation identified from a patient provided us with an opportunity to examine the consequences of a full-length, functionally compromised, protein product on neuronal structure and function. Using primary hippocampal neurons, we now report that NHE6<sub>AES</sub>-mCh puncta localize less to early and recycling endosomes and more to acidic late endosomes and lysosomes when compared to NHE6<sub>WT</sub>-mCh. Incidentally, through additional immunocytochemistry experiments probing for GM2 ganglioside accumulation, which are indicative of endolysosomal dysfunction and observed in certain brain areas of NHE6 KO mice (Strømme et al., 2011), we have no reason to believe that acute transfection of NHE6 constructs compromised

lysosomal function in our neurons (data not shown).

NHE6<sub>AES</sub>-mCh transfection significantly decreased dendritic spine density compared to controls, paralleling previous observations of hippocampal neurons from NHE6 KO mice (Ouyang et al., 2013). Spine morphology is typically correlated with AMPAR density and post-synaptic density (PSD) size, and thus spine size is a common measure of synaptic strength and stability (Phillips and Pozzo-Miller, 2015). As such, the observed reduction in the density of larger mushroom-type spines in neurons expressing NHE6 $_{\Delta ES}$ -mCh is indicative of a reduction in excitatory synaptic neurotransmission and proper neuronal circuit connectivity, as even minimal shifts in spine size are associated with significant changes in synaptic function at both the cellular and circuit levels (Forrest et al., 2018). Indeed, disruptions in spine density, size, and stability are common to a number of neurodevelopmental disorders that present with cognitive impairment, including Angelman, Rett, Fragile X, and Down syndromes (Phillips and Pozzo-Miller, 2015). Interestingly, in Fragile X syndrome and other such disorders involving intellectual disability, post-mortem examinations have revealed a "torturous" spine morphology resulting from an increase in immature filopodia density, similar to our observations (Forrest et al., 2018; Phillips and Pozzo-Miller, 2015). Together, these findings reveal that

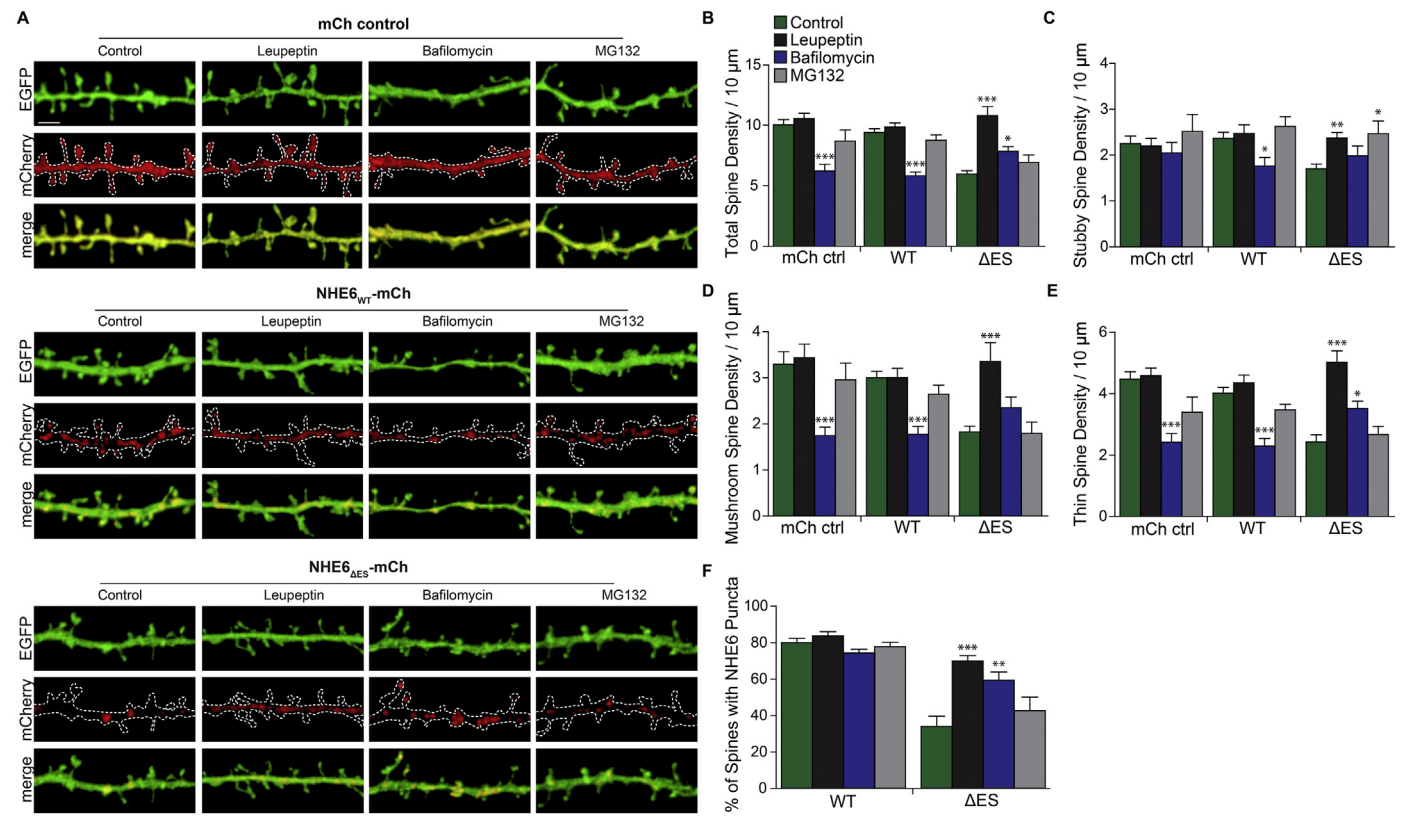


Fig. 7. Inhibitors of lysosomal function, but not proteasomal function, are beneficial for spine density in NHE6 ΔES-transfected neurons. A: Representative confocal micrographs of secondary or tertiary dendrites from transfected primary hippocampal neuron co-transfected with EGFP and mCh alone, NHE6<sub>MT</sub>-mCh or NHE6<sub>ΔES</sub>-mCh and untreated (control) or treated overnight with leupeptin, bafilomycin, or MG132. Channels are shown separately and merged; white outlines denote location of EGFP-positive dendrite. Scale bar:  $2 \,\mu$ m. B-E: Quantification of mean  $\pm$  S.E.M. density of stubby (B), mushroom (C), thin (D), and total (E) spines following each treatment for each transfection condition. F: Quantification of mean  $\pm$  S.E.M. fraction of spines containing puncta of transfected, overexpressed NHE6 WT or ΔES puncta of all spines analyzed for NHE6 WT-mCh and NHE6 ΔES-mCh cells for each treatment condition. For mCh control, control: n = 461 spines along 450.302 μm of dendrite from 16 cells, leupeptin: n = 431 spines along 411.083 μm of dendrite from 14 cells; bafilomycin: n = 199 spines along 316.209 μm of dendrite from 12 cells; MG132: n = 193 spines along 223.232 μm of dendrite from 8 cells. For NHE6 WT, control: n = 440 spines along 469.836 μm of dendrite from 16 cells; bafilomycin: n = 275 spines along 308.887 μm of dendrite from 12 cells; MG132: n = 207 spines along 238.938 μm of dendrite from 8 cells. For NHE6 ΔES, control: n = 275 spines along 459.203 μm of dendrite from 16 cells; leupeptin: n = 460 spines along 443.558 μm of dendrite from 14 cells; bafilomycin: n = 236 spines along 298.703 μm of dendrite from 12 cells; MG132: n = 159 spines along 234.028 μm of dendrite from 8 cells, 10 separate experiments. \*p < .05, \*\*p < .01, \*\*\*p < .001; Dunnett's Multiple Comparison Test.

NHE6 mutants induce deficits in the formation and maintenance of excitatory synapses, which could underlie the learning deficits observed in individuals with CS.

We also observed that NHE6 $_{\Delta ES}$ -mCh-expressing neurons fail to undergo significant structural and functional remodeling in response to gly-ChemLTP stimulation. Increases in spine head volume are a common response to LTP in the hippocampus and cortex and are reflective of recruitment of excitatory postsynaptic machinery to the spine and an increase in synaptic strength (Phillips and Pozzo-Miller, 2015). This is seen predominantly in smaller spines, which are thought to be more labile and plastic than larger, more stable spines. Importantly, it has been shown that recycling endosomes, the pH and function of which are mediated in part by NHE6, provides additional AMPARs and lipid membranes to dendritic spines following LTP induction, thus accounting for the associated changes in synaptic structure and function (Park et al., 2004; Petrini et al., 2009). We thus postulate that the inability of smaller, thin-type spines to enlarge in  $\Delta ES$ -transfected cells results from impaired trafficking mechanisms that normally regulate structural plasticity mechanisms. Likewise, NHE6<sub>AES</sub>-mCh-transfected neurons also had significantly fewer spine-localized GluA1 puncta and failed to recruit additional AMPARs to these spines following gly-ChemLTP stimulation. This resulted in a functional change at the synapse: specifically,  $\Delta$ ES-expressing cells failed to show the expected increase in mEPSC amplitude in response to gly-ChemLTP-stimulation,

as seen in controls. Given that NHE6 normally traffics into spine heads alongside GluA1 following gly-ChemLTP (Deane et al., 2013), this suggests that NHE6 plays an essential role in AMPAR trafficking mechanisms at the synapse. It should be noted that NHE6 is found extensively within excitatory postsynaptic compartments, with significant trafficking to the base and head regions of spines. We and others have also shown that the endocytosis of certain integral plasma membrane proteins is regulated by NHE6 function (Ilie et al., 2016; Ilie et al., 2014; Ohgaki et al., 2010). Therefore, we hypothesize that NHE6 specifically participates in the maintenance of endocytic zones, which are located adjacent to PSDs and contain machinery necessary to internalize AMPARs into endosomes and maintain them close to the synapse. In response to LTP induction, this pool of recycling endosomes is then important for the addition of both AMPARs and additional lipid membrane to spine heads to mediate their enlargement and functional potentiation (Park et al., 2006; Rácz et al., 2004; Yudowski et al., 2007). As such, Petrini and colleagues reported that impairing AMPAR recycling through endocytic zones by interfering with endocytic machinery diminishes the number of PSD-localized AMPARs (Petrini et al., 2009). Likewise, we postulated that synaptic AMPAR recycling in  $\Delta$ EStransfected neurons is impaired by the overacidification of endosomes containing GluA1-positive AMPARs, which increases the likelihood the receptors will be erroneously targeted to and degraded within lysosomes (Fig. 9I). Overall, it follows that impairments in structural and

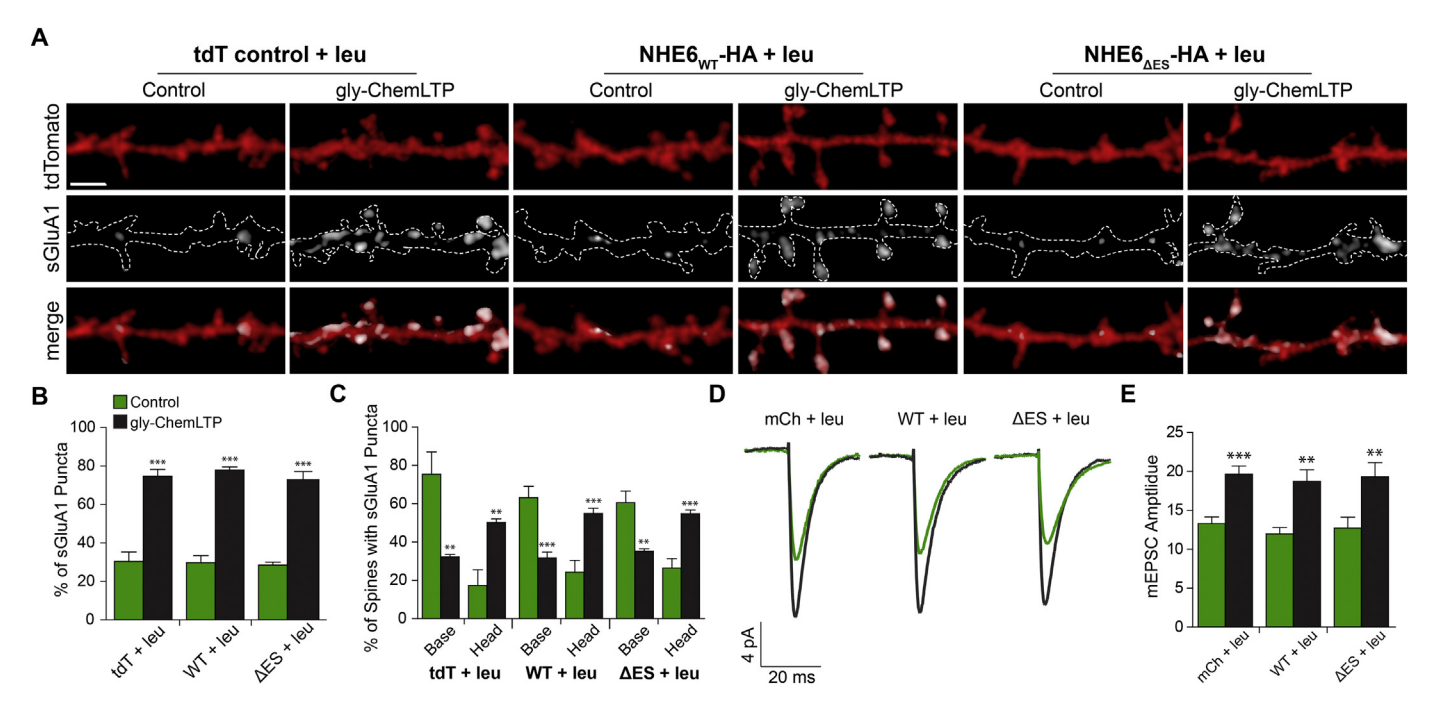


Fig. 8. Leupeptin, a lysosomal protease inhibitor, restores the functional response to gly-ChemLTP in NHE6  $\Delta$ ES-transfected neurons. A: Representative confocal micrographs of secondary or tertiary dendrites from leupeptin-treated primary hippocampal neurons that were either unstimulated (control) or stimulated (gly-ChemLTP) for each transfection condition and stained for surface SEP-GluA1 (sGluA1) under non-permeabilizing conditions. Channels are shown separately and merged; white outlines denote location of tdTomato-positive dendrite. Scale bar:  $2 \mu m$ . B: Mean  $\pm$  S.E.M. percentage of spines containing sGluA1 puncta for control and gly-ChemLTP conditions for each transfection condition. C: Mean  $\pm$  S.E.M. proportion of sGluA1 puncta in each spine subregion for control and gly-ChemLTP-stimulated, leupeptin-treated cultures. For mCh + leu, control: n = 155 spines along 189.456  $\mu$ m of dendrite from 7 cells; gly-ChemLTP: n = 131 spines along 179.799  $\mu$ m of dendrite from 7 cells; for NHE6 WT + leu, control: n = 120 spines along 166.109  $\mu$ m of dendrite from 7 cells, gly-ChemLTP: n = 150 spines along 179.799  $\mu$ m of dendrite from 7 cells; for NHE6  $\Delta$ ES + leu, control: 104 spines along 174.24  $\mu$ m of dendrite from 7 cells; gly-ChemLTP: n = 101 spines along 164.519  $\mu$ m of dendrite from 7 cells, 3 separate experiments. D: Average AMPAR-mEPSC event trace of an unstimulated control and gly-ChemLTP-stimulated cell for each transfection condition with leupeptin pre-treatment. E: Mean  $\pm$  S.E.M. mEPSC amplitude of all cells analyzed under each stimulation and transfection condition with leupeptin pre-treatment. n = 13 cells for each transfection condition, 5 separate experiments. n = 100.001; independent Student's t-test, two-tailed.

functional changes at synaptic sites could arise from  $\Delta$ ES-induced deficiencies in endosomal trafficking mechanisms at the synapse.

Given that the localization of AMPARs is heavily dependent on endosomal trafficking mechanisms, we hypothesized that NHE6 ΔES may lead to an excessive endolysosomal degradation of these receptors. We verified this hypothesis using leupeptin, an inhibitor of cysteine, serine and threonine proteases in the endolysosomal pathway (Monti et al., 1998), and found that in ΔES-expressing neurons, leupeptin restored spine density to levels comparable to controls. Moreover, in  $\Delta ES$ expressing cells that were pre-treated with leupeptin before being subjected to LTP induction, the spines were enlarged and were able to recruit GluA1-containing AMPARs; these cells underwent functional potentiation as well. Thus, the loss of NHE6 function may indeed favour both enhanced endolysosomal trafficking and degradation of AMPARs and other such cargo in hippocampal neurons, subsequently disrupting their signaling. By preventing excessive degradation of GluA1 in  $\Delta$ ES mutants, we were then able to replenish the pool of AMPARs available for insertion into synaptic sites following LTP induction (illustrated in Fig. 9I). Parenthetically, it has been shown that in dorsal root ganglion neurons, 24h leupeptin treatment prevented the ligand-induced degradation of fibroblast growth factor (FGF) receptor 1, enhancing its recycling and thereby promoting axon elongation in these cells (Hausott et al., 2012; Hausott et al., 2008). This finding emphasizes the potential benefit of regulating lysosomal function in neurons to promote changes in their morphology and function. To verify that excessive lysosomal degradation was the result of endosomal overacidification, we rendered endosomes more alkaline by applying bafilomycin, an H+-ATPase inhibitor. Surprisingly, this treatment was detrimental to spine density in both mCh- and NHE6wT-mCh-

transfected neurons. Since bafilomycin blocks acidification of all endomembrane compartments of the secretory and degradative pathways, this detrimental effect may be the result of an overalkalinization of most secretory and endocytic compartments, which then broadly disrupts endomembrane trafficking mechanisms and cellular function. Thus, bafilomycin treatment likely had a more pervasive suppressive effect on organellar dynamics in healthy cells. This observation underpins the importance of regulating organellar pH within a tight range, as both drastic increases and decreases in this parameter can disrupt trafficking mechanisms and cell function (Casey et al., 2010; Paroutis et al., 2004). Conversely, bafilomycin treatment partially restored spine density in NHE6 $_{\Delta ES}$ -mCh-expressing neurons, presumably by limiting excessive acidification and degradation of endosomal cargo under these conditions. Indeed, previous work has demonstrated that bafilomycin treatment can prevent the degradation of internalized receptors in cultured heterologous cells (Yoshimori et al., 1991). Interestingly, while we have shown that NHE6AES-mCh also partially undergoes degradation through proteasomes (Ilie et al., 2016), proteasomal inhibition with MG132 did not rescue spine density in ΔES-expressing neurons. This suggests that specifically limiting excessive endosomal acidification and mistrafficking and degradation of cargo within the lysosome may be a potential strategy to ameliorate some of the deleterious effects induced by the  $\Delta$ ES mutation.

Overall, our results suggest that this mutation in NHE6 can lead to dysregulation of endosomal trafficking and disruption of neuronal morphology and synaptic function. These findings could have important implications for understanding the pathogenesis of other neurological disorders as well. For instance, NHE6 levels have been found to be downregulated in the brains of patients with Alzheimer's disease,

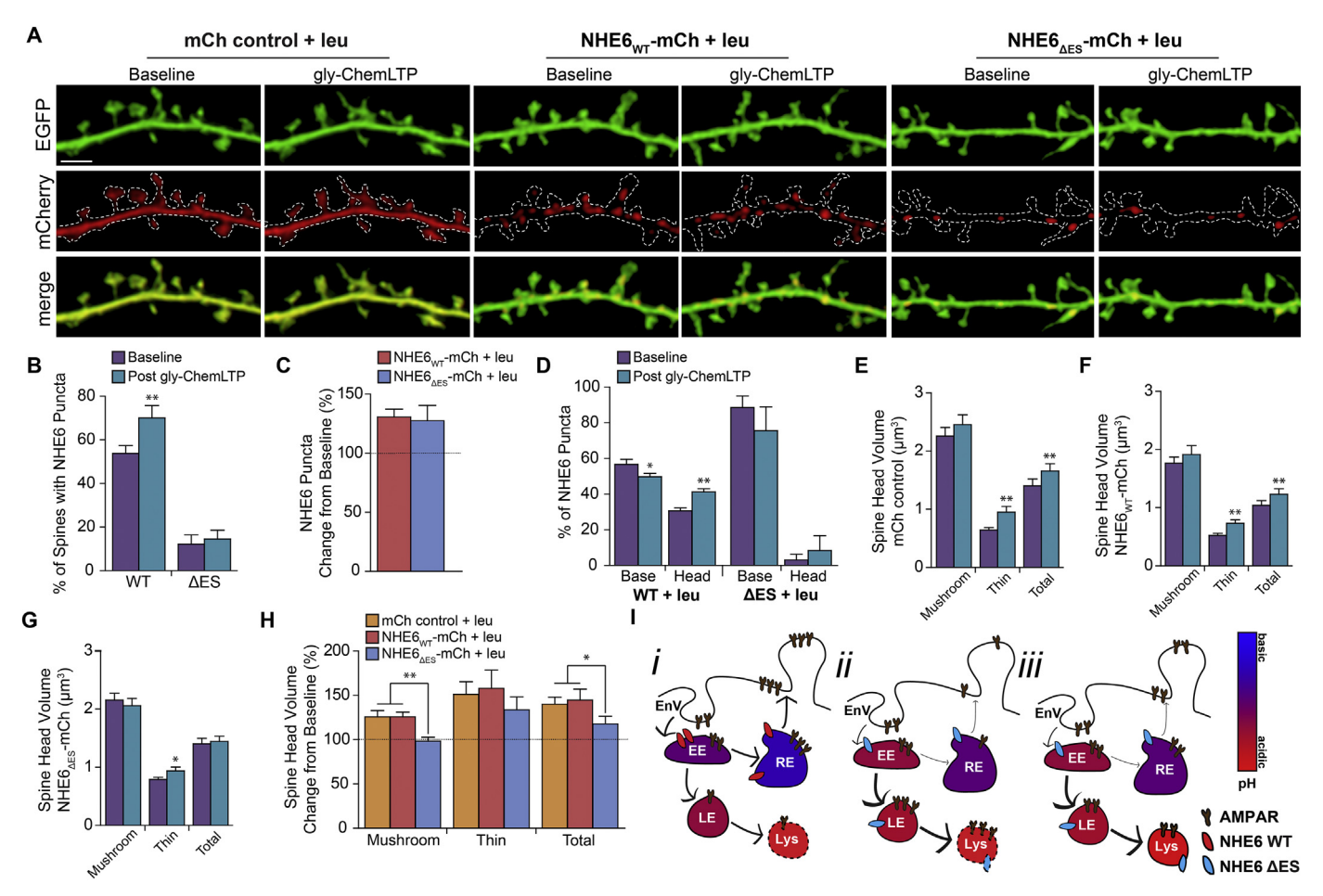


Fig. 9. Leupeptin partially restores the structural response to gly-ChemLTP. A: Representative confocal micrographs of secondary or tertiary dendrites from transfected, leupeptin-treated primary hippocampal neurons at baseline and post gly-ChemLTP for each transfection condition. Channels are shown separately and merged; white outlines denote location of EGFP-positive dendrite. Scale bar:  $3 \mu m$ . B: Mean  $\pm$  S.E.M. percentage of spines containing NHE6 WT or  $\Delta$ ES puncta at baseline and 20 min post gly-ChemLTP following leupeptin pre-treatment. C: Following gly-ChemLTP, the mean  $\pm$  S.E.M. percent change of NHE6 WT or  $\Delta$ ES-positive spines. D: Mean  $\pm$  S.E.M. proportion of NHE6 WT or  $\Delta$ ES puncta in each spine subregion at baseline and following gly-ChemLTP with leupeptin pre-treatment. E-G: Mean  $\pm$  S.E.M. spine head volume measurements for mushroom, thin, and total spines in mCh control- (E), NHE6 WT- (F), and NHE6  $\Delta$ ES- (G)-transfected neurons at baseline and following gly-ChemLTP with leupeptin pre-treatment. H: Following leupeptin pre-treatment and gly-ChemLTP stimulation, the mean  $\pm$  S.E.M. percent change from baseline in spine head volume. For mCh control + leu: 168 spines along 202.54  $\mu$ m of dendrite from 8 cells; NHE6 WT + leu: 225 spines along 231.468  $\mu$ m of dendrite from 8 cells; NHE6  $\Delta$ ES + leu: 185 spines along 227.988  $\mu$ m of dendrite from 8 cells; Separate experiments.  $\mu$  < .05, " $\mu$  < .01; paired Student's t-test, two-tailed (B-D), Wilcoxon signed rank test (E-G), Kruskal-Wallis test with Dunn's Multiple Comparison test (H). I: Representative schematic. Under normal conditions with NHE6 WT (i), internalized cargo, such as AMPARs, are preferentially recycled back to perisynaptic zones. However, with NHE6  $\Delta$ ES (ii), AMPARs are instead targeted to the late endosome and lysosome and subsequently degraded, decreasing their availability at synaptic sites. With leupeptin treatment (iii), this aberrant lysosomal degradation is prevented, thereby allowing for these AMPARs to be trafficked to the

Parkinson's disease, and autism spectrum disorders (Kondapalli et al., 2014; Prasad and Rao, 2015; Schwede et al., 2013). This suggests that similar mechanisms of endosomal mistrafficking may occur in these pathological states as well. As such, additional studies of NHE6 function and regulation will prove valuable in the development of novel therapeutic strategies for treating cognitive deficits observed in rare disorders such as CS, as well as other common neurodegenerative disorders that affect a more significant proportion of the global population.

#### Ethics approval and consent to participate

All animal handling procedures were carried out following the guidelines established by the Canadian Council on Animal Care and were approved by the Animal Resource Committee of the School of Medicine at McGill University, as outlined in McGill University Animal Handling Protocol #5057.

#### Availability of data and material

All data generated or analyzed during this study are included in this published article and its supplementary information files. Additional file 1: Fig. S1: Dominant negative effect upon endogenous WT NHE6 trafficking into dendrites following  $\Delta$ ES transfection. Fig. S2: NMDAR dependence of gly-ChemLTP stimulation. Tables S1–11: raw values for data presented in Figs. 1–9 and S1–2.

#### **Competing interests**

The authors declare no competing interests.

#### Funding

RAM was supported by the Canadian Institutes of Health Research (CIHR) (MOP-133611) and the Natural Sciences and Engineering Research Council of Canada (NSERC) (RGPIN 341942-13). JO was supported by CIHR (MOP-111191). RAM and JO were further

supported jointly by CIHR (PJT-155976). AYLG was supported by Alexander Graham Bell Canada Graduate Scholarships from NSERC.

#### Authors' contributions

AYLG generated and analyzed all of the data in the present study and wrote the manuscript. AI designed, generated, and helped to transfect DNA constructs. PKYC helped to collect electrophysiological data. JO and RAM contributed to study design, supervision, and coordination. AYLG and RAM wrote the manuscript; all authors critically discussed, revised, and approved the final manuscript.

#### Acknowledgements

We are grateful to the animal handling services provided by the Comparative Medicine and Animal Resources Centre at the Goodman Cancer Research Centre at McGill University. We also thank Mr. François Charron for his technical support.

#### Appendix A. Supplementary data

Supplementary data to this article can be found online at https://doi.org/10.1016/j.nbd.2019.104490.

#### References

- Brett, C.L., Wei, Y., Donowitz, M., Rao, R., 2002. Human Na(+)/H(+) exchanger isoform 6 is found in recycling endosomes of cells, not in mitochondria. Am. J. Phys. Cell Physiol. 282, C1031–C1041. https://doi.org/10.1152/ajpcell.00420.2001.
- Brewer, G.J., Torricelli, J.R., 2007. Isolation and culture of adult neurons and neuro-spheres. Nat. Protoc. 2, 1490–1498. https://doi.org/10.1038/nprot.2007.207.
- Carlsson, S.R., Fukuda, M., 1989. Structure of human lysosomal membrane glycoprotein 1. Assignment of disulfide bonds and visualization of its domain arrangement. J. Biol. Chem. 264, 20526–20531 2584229.
- Casey, J.R., Grinstein, S., Orlowski, J., 2010. Sensors and regulators of intracellular pH. Nat. Rev. Mol. Cell Biol. 11, 50–61. https://doi.org/10.1038/nrm2820.
- Chang, P.K.Y., Prenosil, G.A., Verbich, D., Gill, R., McKinney, R.A., 2014. Prolonged ampakine exposure prunes dendritic spines and increases presynaptic release probability for enhanced long-term potentiation in the hippocampus. Eur. J. Neurosci. 40, 2766–2776. https://doi.org/10.1111/ejn.12638.
- Chater, T.E., Goda, Y., 2014. The role of AMPA receptors in postsynaptic mechanisms of synaptic plasticity. Front. Cell. Neurosci. 8, 1–14. https://doi.org/10.3389/fncel. 2014.0401
- Christianson, A.L., Stevenson, R.E., van der Meyden, C.H., Pelser, J., Theron, F.W., van Rensburg, P.L., Chandler, M., Schwartz, C.E., 1999. X linked severe mental retardation, craniofacial dysmorphology, epilepsy, ophthalmoplegia, and cerebellar atrophy in a large south African kindred is localised to Xq24-q27. J. Med. Genet. 36, 759–766.
- Davies, J., Evans, R.H., Herrling, P.L., Jones, A.W., Olverman, H.J., Pook, P., Watkins, J.C., 1986. CPP, a new potent and selective NMDA antagonist. Depression of central neuron responses, affinity for [3H]d-AP5 binding sites on brain membranes and anticonvulsant activity. Brain Res. 382, 169–173. https://doi.org/10.1016/0006-8993(86)90127-7.
- Deane, E.C., Ilie, A.E., Sizdahkhani, S., Das Gupta, M., Orlowski, J., McKinney, R.A., 2013. Enhanced recruitment of endosomal Na+/H+ exchanger NHE6 into dendritic spines of hippocampal pyramidal neurons during NMDA receptor-dependent longterm potentiation. J. Neurosci. 33, 595–610. https://doi.org/10.1523/JNEUROSCI. 2583-12.2013.
- Ding, J., Rainey, J.K., Xu, C., Sykes, B.D., Fliegel, L., 2006. Structural and functional characterization of transmembrane segment VII of the Na+/H+ exchanger isoform 1. J. Biol. Chem. 281, 29817–29829. https://doi.org/10.1074/jbc.M606152200.
- Forrest, M.P., Parnell, E., Penzes, P., 2018. Dendritic structural plasticity and neuropsychiatric disease. Nat. Rev. Neurosci. 19, 215–234. https://doi.org/10.1038/nrn. 2018.16.
- Fortin, D.A., Davare, M.A., Srivastava, T., Brady, J.D., Nygaard, S., Derkach, V.A., Soderling, T.R., 2010. Long-term potentiation-dependent spine enlargement requires synaptic Ca2+-permeable AMPA receptors recruited by CaM-kinase I. J. Neurosci. 30, 11565–11575. https://doi.org/10.1523/JNEUROSCI.1746-10.2010.
- Garbern, J.Y., Neumann, M., Trojanowski, J.Q., Lee, V.M.-Y., Feldman, G., Norris, J.W., Friez, M.J., Schwartz, C.E., Stevenson, R., Sima, A.A., 2010. A mutation affecting the sodium/proton exchanger, SLC9A6, causes mental retardation with tau deposition. Brain 133, 1391–1402. https://doi.org/10.1093/brain/awq071.
- Gilfillan, G.D., Selmer, K.K., Roxrud, I., Smith, R., Kyllerman, M., Eiklid, K., Kroken, M., Mattingsdal, M., Egeland, T., Stenmark, H., Sjøholm, H., Server, A., Samuelsson, L., Christianson, A., Tarpey, P., Whibley, A., Stratton, M.R., Futreal, P.A., Teague, J., Edkins, S., Gecz, J., Turner, G., Raymond, F.L., Schwartz, C., Stevenson, R.E., Undlien, D.E., Strømme, P., 2008. SLC9A6 mutations cause X-linked mental retardation, microcephaly, epilepsy, and ataxia, a phenotype mimicking Angelman syndrome. Am. J. Hum. Genet. 82, 1003–1010. https://doi.org/10.1016/j.ajhg.2008.

- 01.013
- Grant, B.D., Donaldson, J.G., 2009. Pathways and mechanisms of endocytic recycling. Nat. Rev. Mol. Cell Biol. 10, 597–608. https://doi.org/10.1038/nrm2755.
- Harris, K.M., Jensen, F.E., Tsao, B., 1992. Three-dimensional structure of dendritic spines and synapses in rat hippocampus (CA1) at postnatal day 15 and adult ages: implications for the maturation of synaptic physiology and long-term potentiation. J. Neurosci. 12, 2685–2705.
- Hausott, B., Schlick, B., Vallant, N., Dorn, R., Klimaschewski, L., 2008. Promotion of neurite outgrowth by fibroblast growth factor receptor 1 overexpression and lysosomal inhibition of receptor degradation in pheochromocytoma cells and adult sensory neurons. Neuroscience 153, 461–473. https://doi.org/10.1016/j.neuroscience. 2008.01.083.
- Hausott, B., Vallant, N., Hochfilzer, M., Mangger, S., Irschick, R., Haugsten, E.M., Klimaschewski, L., 2012. Leupeptin enhances cell surface localization of fibroblast growth factor receptor 1 in adult sensory neurons by increased recycling. Eur. J. Cell Biol. 91, 129–138. https://doi.org/10.1016/j.ejcb.2011.09.009.
- Ilie, A., Weinstein, E., Boucher, A., McKinney, R.A., Orlowski, J., 2014. Impaired post-translational processing and trafficking of an endosomal Na+/H+ exchanger NHE6 mutant (Δ(370)WST(372)) associated with X-linked intellectual disability and autism. Neurochem. Int. 73, 192–203. https://doi.org/10.1016/j.neuint.2013.09.
- Ilie, A., Gao, A.Y.L., Reid, J., Boucher, A., Barriere, H., McEwan, C., Lukacs, G., Mckinney, R.A., Orlowski, J., 2016. A Christianson syndrome-linked deletion mutation (A287ES288) in SLC9A6 disrupts recycling endosomal function and induces neuro-degeneration and cell death. Mol. Neurodegener. 1–28. https://doi.org/10.1186/s13024-016-0129-9.
- Jiang, M., Chen, G., 2006. High Ca2+-phosphate transfection efficiency in low-density neuronal cultures. Nat. Protoc. 1, 695–700. https://doi.org/10.1038/nprot.2006.86.
- Koleske, A.J., 2013. Molecular mechanisms of dendrite stability. Nat. Rev. Neurosci. 14, 536–550. https://doi.org/10.1038/nrn3486.
- Kondapalli, K.C., Prasad, H., Rao, R., 2014. An inside job: how endosomal Na(+)/H(+) exchangers link to autism and neurological disease. Front. Cell. Neurosci. 8, 172. https://doi.org/10.3389/fncel.2014.00172.
- Lynch, M.A., 2004. Long-term potentiation and memory. Physiol. Rev. 84, 87–136. https://doi.org/10.1152/physrev.00014.2003.
- Malenka, R.C., Nicoll, R.A., 1999. Long-term potentiation a decade of progress? Science (80-) 285, 1870–1874. https://doi.org/10.1126/science.285.5435.1870.
- Maxfield, F.R., McGraw, T.E., 2004. Endocytic recycling. Nat. Rev. Mol. Cell Biol. 5, 121-132. https://doi.org/10.1038/nrm1315.
- McKinney, R.A., 2010. Excitatory amino acid involvement in dendritic spine formation, maintenance and remodelling. J. Physiol. 588, 107–116. https://doi.org/10.1113/ jphysiol.2009.178905.
- Mellman, I., Fuchs, R., Helenius, A., 1986. Acidification of the endocytotic and exocytic pathways. Annu. Rev. Biochem. 55, 663–700.
- Monti, B., Sparapani, M., Contestabile, A., 1998. Differential toxicity of protease inhibitors in cultures of cerebellar granule neurons. Exp. Neurol. 153, 335–341. S0014-4886(98)96858-3 [pii]. https://doi.org/10.1006/exnr.1998.6858.
- Mu, F.-T., Callaghan, J.M., Steele-Mortimer, O., Stenmark, H., Parton, R.G., Campbell, P.L., McCluskey, J., Yeo, J.-P., Tock, E.P.C., Toh, B.-H., 1995. EEA1, an early endosome-associated protein. J. Biol. Chem. 13503–13511. https://doi.org/10.1074/jbc.270.22.13503.
- Nakamura, N., Tanaka, S., Teko, Y., Mitsui, K., Kanazawa, H., 2005. Four Na+/H+ exchanger isoforms are distributed to Golgi and post-Golgi compartments and are involved in organelle pH regulation. J. Biol. Chem. 280, 1561–1572. https://doi.org/10.1074/jbc.M410041200.
- Numakawa, T., Suzuki, S., Kumamaru, E., Adachi, N., Richards, M., Kunugi, H., 2010. BDNF function and intracellular signaling in neurons. Histol. Histopathol. 25, 237–258.
- Ohgaki, R., Matsushita, M., Kanazawa, H., Ogihara, S., Hoekstra, D., van Ijzendoorn, S.C.D., 2010. The Na+/H+ exchanger NHE6 in the endosomal recycling system is involved in the development of apical bile canalicular surface domains in HepG2 cells. Mol. Biol. Cell 21, 1293–1304. https://doi.org/10.1091/mbc.E09-09-0767.
- Orlowski, J., Grinstein, S., 2011. Na+/H+ exchangers. Comp. Physiol. 1, 2083–2100. https://doi.org/10.1002/cphy.c110020.
- Ouyang, Q., Lizarraga, S.B., Schmidt, M., Yang, U., Gong, J., Ellisor, D., Kauer, J.A., Morrow, E.M., 2013. Christianson syndrome protein NHE6 modulates TrkB endosomal signaling required for neuronal circuit development. Neuron 80, 97–112. https://doi.org/10.1016/j.neuron.2013.07.043.
- Overly, C.C., Hollenbeck, P.J., 1996. Dynamic organization of endocytic pathways in axons of cultured sympathetic neurons. J. Neurosci. 16, 6056–6064 (doi:1996/10/01 00:01).
- Park, M., Penick, E.C., Edwards, J.G., Kauer, J.A., Ehlers, M.D., 2004. Recycling endosomes supply AMPA receptors for LTP. Science 305, 1972–1975. https://doi.org/10. 1126/science.1102026.
- Park, M., Salgado, J.M., Ostroff, L., Helton, T.D., Camenzind, G., Harris, K.M., Ehlers, M.D., Augusta, G., 2006. Plasticity-induced growth of dendritic spines by exocytic trafficking from recycling endosomes. Neuron 52, 817–830.
- Paroutis, P., Touret, N., Grinstein, S., 2004. The pH of the secretory pathway: measurement, determinants, and regulation. Physiology (Bethesda) 19, 207–215. https://doi.org/10.1152/physiol.00005.2004.
- Pescosolido, M.F., Stein, D.M., Schmidt, M., Moufawad El Achkar, C., Sabbagh, M., Rogg, J.M., Tantravahi, U., McLean, R.L., Liu, J.S., Poduri, A., Morrow, E.M., 2014. Genetic and phenotypic diversity of NHE6 mutations in Christianson syndrome. Ann. Neurol. 581–593. https://doi.org/10.1002/ana.24225.
- Petrini, E.M., Lu, J., Cognet, L., Lounis, B., Ehlers, M.D., Choquet, D., 2009. Endocytic trafficking and recycling maintain a pool of mobile surface AMPA receptors required

- for synaptic potentiation. Neuron 63, 92–105. https://doi.org/10.1016/j.neuron.
- Phillips, M., Pozzo-Miller, L., 2015. Dendritic spine dysgenesis in autism related disorders. Neurosci. Lett. 1, 11. https://doi.org/10.1016/j.neulet.2015.01.011.
- Potter, S.M., DeMarse, T.B., 2001. A new approach to neural cell culture for long-term studies. J. Neurosci. Methods 110, 17–24. https://doi.org/10.1016/S0165-0270(01) 00412-5
- Prasad, H., Rao, R., 2015. The Na+/H+ exchanger NHE6 modulates endosomal pH to control processing of amyloid precursor protein in a cell culture model of Alzheimer disease. J. Biol. Chem. https://doi.org/10.1074/jbc.M114.602219.
- Prekeris, R., Klumperman, J., Chen, Y.A., Scheller, R.H., 1998. Syntaxin 13 mediates cycling of plasma membrane proteins via tubulovesicular recycling endosomes. J. Cell Biol. 143, 957–971. https://doi.org/10.1083/jcb.143.4.957.
- Rácz, B., Blanpied, T.A., Ehlers, M.D., Weinberg, R.J., 2004. Lateral organization of endocytic machinery in dendritic spines. Nat. Neurosci. 7, 917–918. https://doi.org/10.1038/nn1303.
- Schroer, R.J., Holden, K.R., Tarpey, P.S., Matheus, M.G., Griesemer, D.A., Friez, M.J., Fan, J.Z., Simensen, R.J., Strømme, P., Stevenson, R.E., Stratton, M.R., Schwartz, C.E., 2010. Natural history of Christianson syndrome. Am. J. Med. Genet. A 152A, 2775–2783. https://doi.org/10.1002/ajmg.a.33093.
- Schwede, M., Garbett, K., Mirnics, K., Geschwind, D.H., Morrow, E.M., 2013. Genes for endosomal NHE6 and NHE9 are misregulated in autism brains. Mol. Psychiatry 19, 1–3. https://doi.org/10.1038/mp.2013.28.
- Selcher, J.C., Xu, W., Hanson, J.E., Malenka, R.C., Madison, D.V., 2012. Glutamate receptor subunit GluA1 is necessary for long-term potentiation and synapse unsilencing, but not long-term depression in mouse hippocampus. Brain Res. 1435, 8–14. https://doi.org/10.1016/j.brainres.2011.11.029.
- Sorra, K.E., Harris, K.M., 2000. Overview on the structure, composition, function, development, and plasticity of hippocampal dendritic spines. Hippocampus 10, 501–511. https://doi.org/10.1002/1098-1063(2000)10:5<501::AID-HIPO1>3.0. CO:2-T.
- Strømme, P., Dobrenis, K., Sillitoe, R.V., Gulinello, M., Ali, N.F., Davidson, C., Micsenyi, M.C., Stephney, G., Ellevog, L., Klungland, A., Walkley, S.U., 2011. X-linked Angelman-like syndrome caused by Slc9a6 knockout in mice exhibits evidence of endosomal-lysosomal dysfunction. Brain 134, 3369–3383. https://doi.org/10.1093/brain/awr250.
- Takahashi, Y., Hosoki, K., Matsushita, M., Funatsuka, M., Saito, K., Kanazawa, H., Goto, Y.-I., Saitoh, S., 2011. A loss-of-function mutation in the SLC9A6 gene causes X-linked mental retardation resembling Angelman syndrome. Am. J. Med. Genet. B Neuropsychiatr. Genet. 156B, 799–807. https://doi.org/10.1002/ajmg.b.31221.
- Tarpey, P.S., Smith, R., Pleasance, E., Whibley, A., Edkins, S., Hardy, C., O'Meara, S., Latimer, C., Dicks, E., Menzies, A., Stephens, P., Blow, M., Greenman, C., Xue, Y., Tyler-Smith, C., Thompson, D., Gray, K., Andrews, J., Barthorpe, S., Buck, G., Cole, J., Dunmore, R., Jones, D., Maddison, M., Mironenko, T., Turner, R., Turrell, K., Varian,

- J., West, S., Widaa, S., Wray, P., Teague, J., Butler, A., Jenkinson, A., Jia, M., Richardson, D., Shepherd, R., Wooster, R., Tejada, M.I., Martinez, F., Carvill, G., Goliath, R., de Brouwer, A.P.M., van Bokhoven, H., Van Esch, H., Chelly, J., Raynaud, M., Ropers, H.-H., Abidi, F.E., Srivastava, A.K., Cox, J., Luo, Y., Mallya, U., Moon, J., Parnau, J., Mohammed, S., Tolmie, J.L., Shoubridge, C., Corbett, M., Gardner, A., Haan, E., Rujirabanjerd, S., Shaw, M., Vandeleur, L., Fullston, T., Easton, D.F., Boyle, J., Partington, M., Hackett, A., Field, M., Skinner, C., Stevenson, R.E., Bobrow, M., Turner, G., Schwartz, C.E., Gecz, J., Raymond, F.L., Futreal, P.A., Stratton, M.R., 2009. A systematic, large-scale resequencing screen of X-chromosome coding exons in mental retardation. Nat. Genet. 41, 535–543. https://doi.org/10.1038/ng.367.
- Vanlandingham, P.A., Ceresa, B.P., 2009. Rab7 regulates late endocytic trafficking downstream of multivesicular body biogenesis and cargo sequestration. J. Biol. Chem. 284, 12110–12124. https://doi.org/10.1074/jbc.M809277200.
- Verma, V., Bali, A., Singh, N., Jaggi, A.S., 2015. Implications of sodium hydrogen exchangers in various brain diseases. J. Basic Clin. Physiol. Pharmacol. 26, 417–426. https://doi.org/10.1515/jbcpp-2014-0117.
- Weisz, O.A., 2003. Acidification and protein traffic. Int. Rev. Cytol. https://doi.org/10. 1016/S0074-7696(03)01005-2.
- Willingham, M.C., Hanover, J.A., Dickson, R.B., Pastan, I., 1984. Morphologic characterization of the pathway of transferrin endocytosis and recycling in human KB cells. Proc. Natl. Acad. Sci. U. S. A. 81, 175–179. https://doi.org/10.1073/pnas.81.1.175
- Xinhan, L., Matsushita, M., Numaza, M., Taguchi, A., Mitsui, K., Kanazawa, H., 2011. Na +/H+ exchanger isoform 6 (NHE6/SLC9A6) is involved in clathrin-dependent endocytosis of transferrin. Am. J. Phys. Cell Physiol. 301, C1431–C1444. https://doi. org/10.1152/ajpcell.00154.2011.
- Xu, M., Ouyang, Q., Gong, J., Pescosolido, M.F., Pruett, B.S., Mishra, S., Schmidt, M., Jones, R.N., Gamsiz Uzun, E.D., Lizarraga, S.B., Morrow, E.M., 2017. Mixed neuro-developmental and neurodegenerative pathology in *Nhe6* -null mouse model of Christianson syndrome. Eneuro(6), ENEURO.0388-17.2017. https://doi.org/10.1523/ENEURO.0388-17.2017.
- Yamashiro, D.J., Maxfield, F.R., 1984. Acidification of endocytic compartments and the intracellular pathways of ligands and receptors. J. Cell. Biochem. https://doi.org/10. 1002/jcb.240260404.
- Yoshimori, T., Yamamoto, A., Moriyama, Y., Futai, M., Tashiro, Y., 1991. Bafilomycin-a1, a specific inhibitor of vacuolar-type H+-atpase, inhibits acidification and protein-degradation in lysosomes of cultured-cells. J. Biol. Chem. 266, 17707–17712.
- Yudowski, G.A., Puthenveedu, M.A., Leonoudakis, D., Panicker, S., Thorn, K.S., Beattie, E.C., von Zastrow, M., 2007. Real-time imaging of discrete exocytic events mediating surface delivery of AMPA receptors. J. Neurosci. 27, 11112–11121. https://doi.org/10.1523/JNEUROSCI.2465-07.2007.
- Zhao, H., Carney, K.E., Falgoust, L., Pan, J.W., Sun, D., Zhang, Z., 2016. Emerging roles of Na +/H + exchangers in epilepsy and developmental brain disorders. Prog. Neurobiol. https://doi.org/10.1016/j.pneurobio.2016.02.002.